The Seasonal Cycle of Stationary Planetary Waves in the Southern Stratosphere: A Numerical Study

by

Volkmar Wirth

Physik Diplom
Universität Bonn
(1987)

Submitted to the Department of Earth, Atmospheric, and Planetary Sciences
in Partial Fulfillment of the Requirements for the Degree of

Master of Science in Meteorology

at the

Massachusetts Institute of Technology

May 1990

Signature of Author: _____

Department of Earth, Atmospheric, and Planetary Sciences
11 May 1990

Certified by: _____

R. Alan Plumb, Professor of Meteorology, thesis supervisor

Accepted by: _____

Tom Jordan, Chairman, Departmental Commitee
on Graduate Students

The Seasonal Cycle of Stationary Planetary Waves in the Southern Stratosphere: A Numerical Study

by

Volkmar Wirth

Submitted to the Department of Earth, Atmospheric, and Planetary Sciences on 11 May 1990 in Partial Fulfillment of the Requirements for the Degree of Master of Science in Meteorology

Abstract

Stationary planetary waves in the southern stratosphere display a characteristic seasonal cycle with two maxima in early and late winter and a relative minimum in midwinter. Previous research suggests that this behaviour is mainly determined by seasonally varying transmission properties of the atmosphere with respect to wave propagation. A related question is whether the index of refraction adequately diagnoses the seasonal cycle in wave propagation. In the present thesis these issues are investigated with the help of a hemispheric, linear, quasigeostrophic model, which prescribes the wave at the top of the troposphere and solves for the wave in the stratosphere.

The model reproduces well the observed overall amplitude and phase behaviour including the direction of wave activity propagation. It is internally consistent in that the upper stratospheric wave can be qualitatively diagnosed using the refractive index. Certain low altitude features of the refractive index turn out to be important. A sensitivity study reveals that mainly the variation in zonal winds and less the variation in forcing contributes to the seasonal wave cycle. Wave response and refractive index are quite sensitive to variations in the zonal wind field at low altitudes and to such variations that change the jet structure of the wind field.

However, despite its internal consistency, the model fails to simulate more detailed features of the observed wave. In particular it does *not* reproduce the observed midwinter minimum in the wave's seasonal cycle. It therefore remains unclear from this study to what degree the latter is determined by wave transmission properties alone.

Thesis Supervisor: R. Alan Plumb
Title: Professor of Meteorology

Acknowledgements

I would like to thank Professor R. Alan Plumb for being such a wonderful teacher and thesis advisor. He was the first to introduce me into the area of dynamical meteorology and he drew my attention to the issues which I worked on for the present master thesis. Without his constant advice, critical suggestions and support this work would not have been possible.

Similarly I want to take this opportunity to thank Professor R. S. Lindzen, who in his both patient and demanding way taught me much of what I learned during the past two years.

I am grateful for help and encouragement from my fellow students and for many stimulating discussions. Special thanks is due to the never-ending kindness and help of Jane McNabb and Tracey Stanelun, who made my life as a graduate student at M.I.T. smooth and trouble-free.

Finally I want to thank all my friends for adding to my time at M.I.T. something which reaches beyond science.

This work was supported by NASA grant # NAGW-1727 and NSF grant # 8911459-ATM.

Contents

Chapter 1

Introduction

Stationary planetary waves in the middle atmosphere show a certain seasonal behaviour. To first approximation there is absence of wave activity in the summer hemisphere (which is characterized by easterly zonal mean winds), whereas one does observe waves of low wavenumbers in the winter hemisphere (which is characterized by westerly zonal mean winds). A qualitative explanation of this behaviour is contained in the pioneering work of Charney and Drazin (1961). In their quasigeostrophic, linear beta-plane model with constant mean zonal wind, it turnes out that vertical stationary wave propagation is possible only for waves of low wavenumbers and for westerly, but not too strong westerly mean winds. This is referred to as the *Charney-Drazin criterion.*

Since the work by Charney and Drazin, propagation of planetary waves has been the focus of numerous studies. Matsuno (1970) investigated propagation of waves forced from a spherical lower boudary in a quasigeostrophic model allowing for both vertical and meridional propagation. He introduced the *refractive index* as a quantity for diagnosing the mean wind field with respect to the possibility for wave propagation. The refractive index proved useful as a qualitative diagnostic tool in several circumstances, even though its application involves the WKB assumption, which does not hold strictly speaking. The diagnostic aspects were elaborated by Karoly and Hoskins (1982), who considered the concept of ray paths and group velocity. They emphasized the importance of meridional (in addition to vertical) wave propagation and demonstrated the important impact of spherical geometry and meridional basic state wind shear on wave propagation. Similarly, Ben-Da Lin

(1982) demonstrated the essential rôle of the polar night jet for wave propagation and the usefullness of the refractive index as a diagnostic tool. The strong sensitivity of stationary planetary waves with respect to basic state variations in a linear model was pointed out by e.g. Schoeberl and Geller (1977) and Nigam and Lindzen (1989).

The main thrust of these studies was the Northern Hemisphere, and most models used some idealized basic state characteristic for the winter atmosphere. This was partly due to the lack of detailed observations. More recently better global atmospheric circulation statistics has become available, in particular for the Southern Hemisphere (e.g. Randel, 1987a). From these data noticeable *differences* in the seasonal cycle of the stratospheric circulation *between the two hemispheres* have become apparent (Hirota et al. 1983; Randel, 1988). The midwinter westerly winds are stronger in the southern stratosphere. On the other hand, stationary planetary waves are stronger in the northern stratosphere. In addition, contrary to the northern stratosphere, in the southern stratosphere the wave amplitudes display a pronounced minimum in midwinter, accompanied by two maxima in early and late winter, respectively. A complete explanation of the different behaviour of the two hemispheres should lead to a better understanding of the phenomenon of planetary waves and their rôle in determining the mean circulation (Andrews, 1989).

In fact, A. Plumb (1989a) suggested an explanation for the different seasonal behaviour on both hemispheres. He used a simple beta-plane model, allowing only vertical wave propagation, but accounting for the interaction between wave and mean state. His result can be readily interpreted with the help of the Charney-Drazin criterion. On the Northern Hemisphere the waves are so strong that they interact nonlinearly with the basic state and therefore prevent the westerlies from becoming very strong, which in turn allows the wave's propagation into the middle atmosphere. On the other hand, on the Southern Hemisphere weaker wave forcing results in planetary waves which are weak enough to remain in the linear regime througout the year; therefore the westerlies can grow very strong and thus prevent the wave's propagation into higher altitudes in midwinter. Alan Plumbs calculations, therefore, suggest that the Southern Hemisphere is a much better place than the Northern Hemisphere for studying waves with a *linear* model. The scenario is also supported by the observation that the stratospheric mean circulation is much closer to radiative equilibrium in the Southern Hemisphere than in

the Northern Hemisphere (e.g. Andrews, 1989). The consistent explanation is that only in the Northern Hemisphere wave mean flow interaction forces a noticeable residual mean circulation (see Andrews et al., 1987, and references therein) and thus drives the system away from thermal equilibrium.

Another possible source of seasonal variation is the varying tropospheric forcing. However, the observed forcing displays comparatively little variation throughout the winter. A. Plumb's model, therefore, suggests the *hypothesis* that the seasonal cycle in the southern stratospheric waves, including the midwinter minimum, is essentially caused by a variation in the wave transmission properties of the atmosphere. If this hypothesis holds, there should be a corresponding seasonal cycle in the refractive index, since the refractive index diagnoses wave propagation. However, observations do not seem to support the latter: the refractive index as derived from data displays no substantial overall variation throughout the winter season (Randel, 1988).

The above discrepancy motivates us to reexamine in the *present study* the seasonal cycle of wave propagation in the Southern Hemisphere more closely. We consider a linear, quasigeostrophic, 2.5–dimensional model, making in particular use of the improved observations. We investigate to what extent the observed seasonal cycle of stationary planetary waves can be explained by the seasonal variation of forcing and zonal mean winds. Taking observed monthly mean zonal mean winds and observed forcing amplitudes as input parameters, the model yields the wave as output. It will turn out that we are able to simulate the gross features of planetary wave propagation and their seasonal cycle. However, the model fails to reproduce the more detailed structure, in particular the midwinter minimum mentioned above. On the other hand, we will show internal consistency within the model in the sense that the model results can be qualitatively understood in terms of refractive index diagnostics. Furthermore we investigate the sensitivity of the model with respect to basic state, forcing and dissipation. It will become clear to what extent the different model features determine the wave's response within the model.

The thesis is organized as follows: First chapter 2 presents the observations relevant to this study. Next in chapter 3 we introduce the model, its basic assumptions and its numerical implementation. Chapter 4 then gives the results of the numerical implementation of the model, and in chapter 5

we study the sensitivity of the model output with respect to the various input parameters. Finally, chapter 6 contains a summary and conclusions.

Chapter 2

Observations

Before we come to describe the model in chapter 3, we give an overview of the observations in the present chapter. Part of the data presented here (the zonal mean flow) is used by the model as input information. The other part (information about the wave) is actually calculated by the model, hence the corresponding observed data serve as the "truth" with which the model output has to be compared. This chapter is kept descriptive and rather short; relevant discussions are deferred to later chapter.

All data are taken from Randel (1987a), which is presumably the best stratospheric climatology currently available. Randel gives a compilation of global atmospheric circulation statistics, ranging from 1000 mb up to 1 mb. The data consist of wind and temperature fields derived from daily geopotential height grids through the years 1979–1986. The climatological monthly mean fields are averages from those eight years. The data originate partly from the NMC operational daily analyses (up to 100 mb), and partly from the Climate Analysis Center section of NMC (above 100 mb). The latter use satellite information in first guess fields. Zonal mean winds are derived from the zonal mean geopotential through the so-called gradient relation. For the zonal Fourier components of the horizontal winds a procedure involving the linearized momentum equations is used. Randel himself analyzed this data set with respect to the seasonal cycle of planetary waves in the Southern Hemisphere (Randel, 1988). Even though we make use exclusively of Randel's data set, it needs to be acknowledged that most of the qualitative features mentioned here were already pointed out earlier by Hirota et al. (1983).

The exact quality of the data is not easy to be assessed. As for the zonal mean zonal wind, the used gradient wind relationship has been shown to be superior to simple geostrophic balance (Randel, 1987b). In general, stratospheric circulation statistics depend on the base-level analysis, which is used to build up the stratospheric height fields from statellite-measured thickness data. Karoly (1987) shows that planetary-scale features in stratospheric height analyses are qualitatively (even though not necessarily quantitatively) insensitive to the base-level analysis. For stationary waves in the *troposphere* Randel (1988) notes that a comparison of his data set with three independent other ones yields an overall excellent agreement. Comparing different independent data sources and analyses specifically for the southern middle atmosphere, Grose and O'Neill (1989) find that the basic fields (temperatures and winds) usually show qualitative agreement. All of this gives some confidence that the qualitative features, which we will refer to in our present study, are real. Additional confidence is provided by the fact that the aforementioned independent analysis by Hirota et al. (1983) agrees in the essential qualitative features with Randel's analysis.

First we present a latitude-time section of the climatological mean zonal winds at the 1 mb level in figure 2.1. The seasonal cycle with westerlies in the winter and easterlies in the summer hemisphere is clearly visible. As mentioned in the introduction, the the midwinter westerlies are considerably stronger in the Southern Hemisphere.

In our present study we concentrate on the months April through October. For these seven months figure 2.2 shows the mean zonal wind in a meridional cross-section. Strong westerlies are established in the southern stratosphere throughout (southern) winter. Wind speeds peak in mid winter, reaching values of about 100 m/sec at the 1 mb level. The core of the so-called polar night jet descends from July till October substantially and shifts poleward. The latter feature is by now observationally well established (see Hartmann et al., 1984, and references therein).

It is important to notice that there is interannual variability in the considered monthly mean fields. Mechoso et al. (1982) show that this is in particular true for the mean zonal winds in July and August. Interannual variability in these months is mostly due to the different timing of the relatively sudden break down of the upper stratospheric jet. This feature gets washed

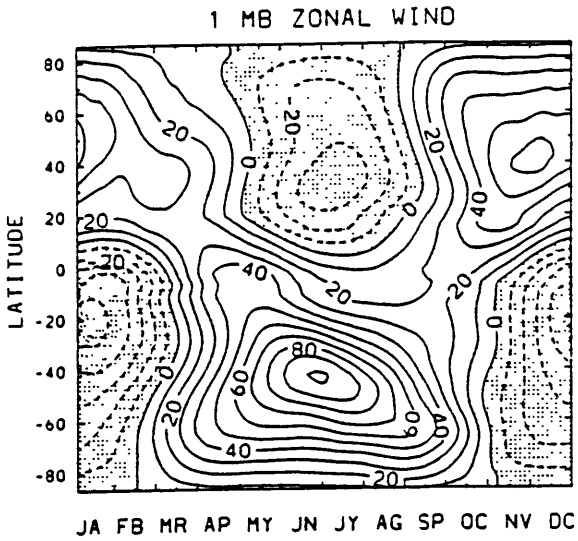

Figure 2.1: Zonal wind (in m/sec) at 1 mb. Latitude-time section. Contour interval: 10 m/sec. Negative values are shaded. Figure taken from Randel (1987a).

out in the present eight year averages.

As for observations of the planeary waves, figure 2.3 gives a latitude-time section of wave amplitude for the stationary wave with zonal wave number 1 at several pressure levels. Obviously, in the middle and high stratosphere the amplitudes are larger in the Northern Hemisphere than in the Southern Hemisphere. Concentrating on the Southern Hemisphere, one can clearly distinguish the two maxima in wave amplitude in early and late winter, and a local minimum in midwinter. This feature is visible throughout the range from 100 mb up to 1 mb. The second maximum is stronger than the first, and the two maxima roughly sandwich the maximum in zonal wind $\bar{u}$. In the higher stratosphere (1 mb level) the wave amplitude maxima and the minimum shift toward earlier months. Comparing the seasonal cycle of the wave in the southern hemispheric higher stratosphere (1 mb panel in figure 2.3) with the seasonal cycle of the zonal wind (figure 2.1), one notices a close correlation between the latitudinal location of the maximum in wave amplitude and that of the westely wind maximum.

Figure 2.4 presents the amplitude of the stationary wave number 1 for consecutive months in a meridional plane. In the lower stratosphere there is a general increase in amplitude with altitude. Some months display an

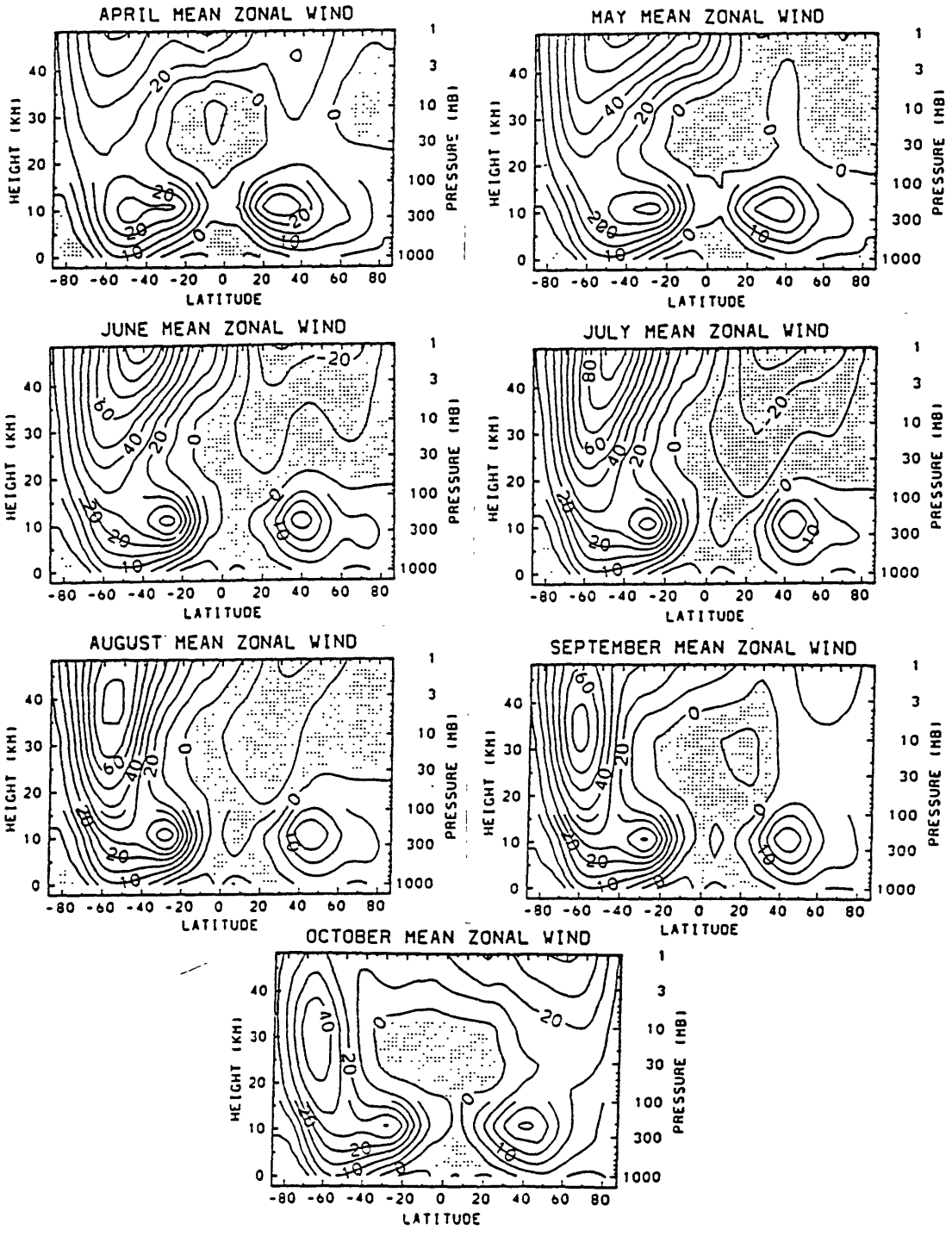

Figure 2.2: Monthly mean zonal mean zonal wind (in m/sec) for the months April through October. Contour interval: 10 m/sec. Negative values are shaded. Meridional section. Figure from Randel (1987a).

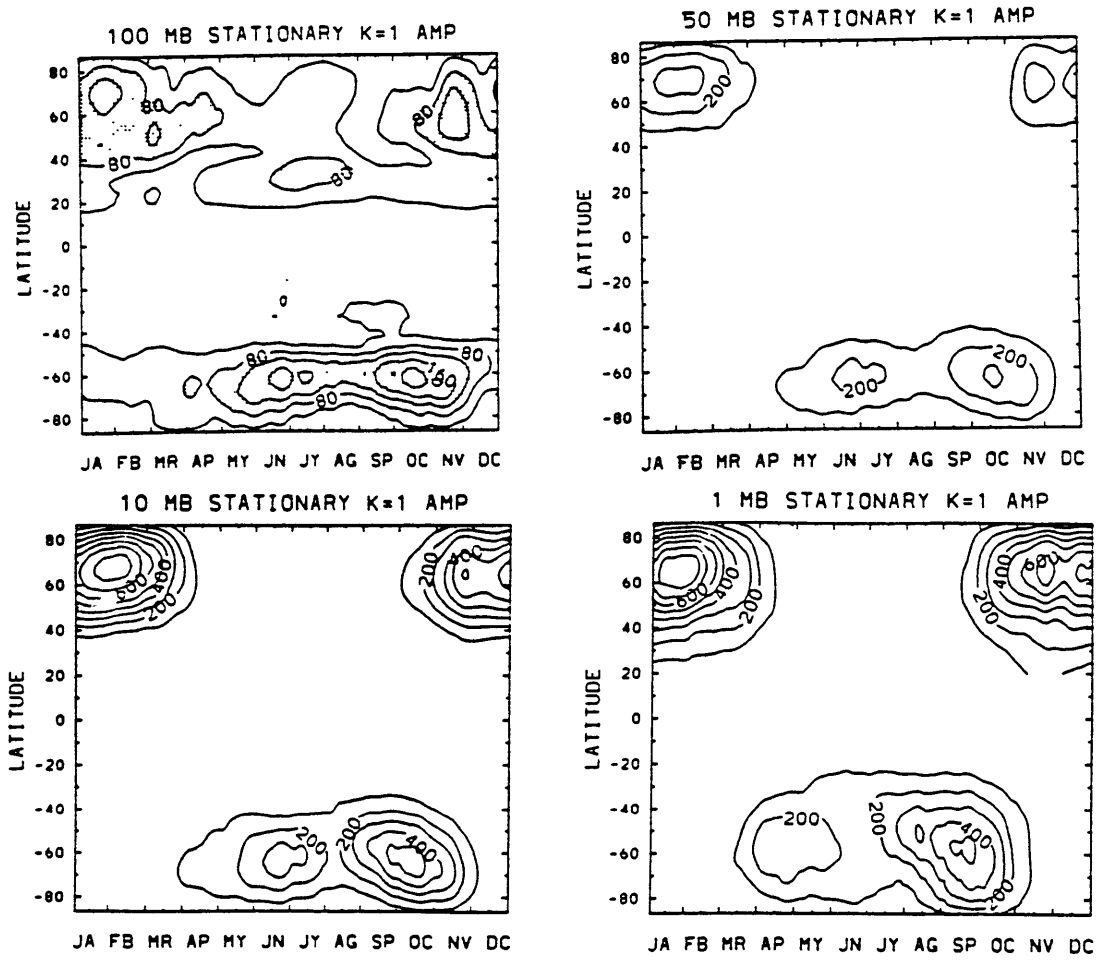

Figure 2.3: Latitude-time section of stationary wave 1 amplitude (in geop. m) at several pressure levels. Contour interval: 40 m at 100 mb, 100 m otherwise. Figure from Randel (1987a).

amplitude maximum in the middle or higher stratosphere. Note that in the later months the amplitude maximum descends and shifts poleward. In this sense the wave's amplitude qualitatively mimics the zonal mean wind (cf. figure 2.2).

The phase structure of the wave 1 shows an interesting and pronounced seasonal cycle (Randel, 1988). Figure 2.5, taken from that reference, gives the longitudinal location of the ridge of the wave at several different pressure levels at 60° southern latitude. Large spacing between the lines indicates strong westward phase tilt with height, and vice versa. Hence, during the time of the first wave maximum (June) the wave has an almost barotropic structure, whereas during the later maximum (September) it is strongly baroclinic.

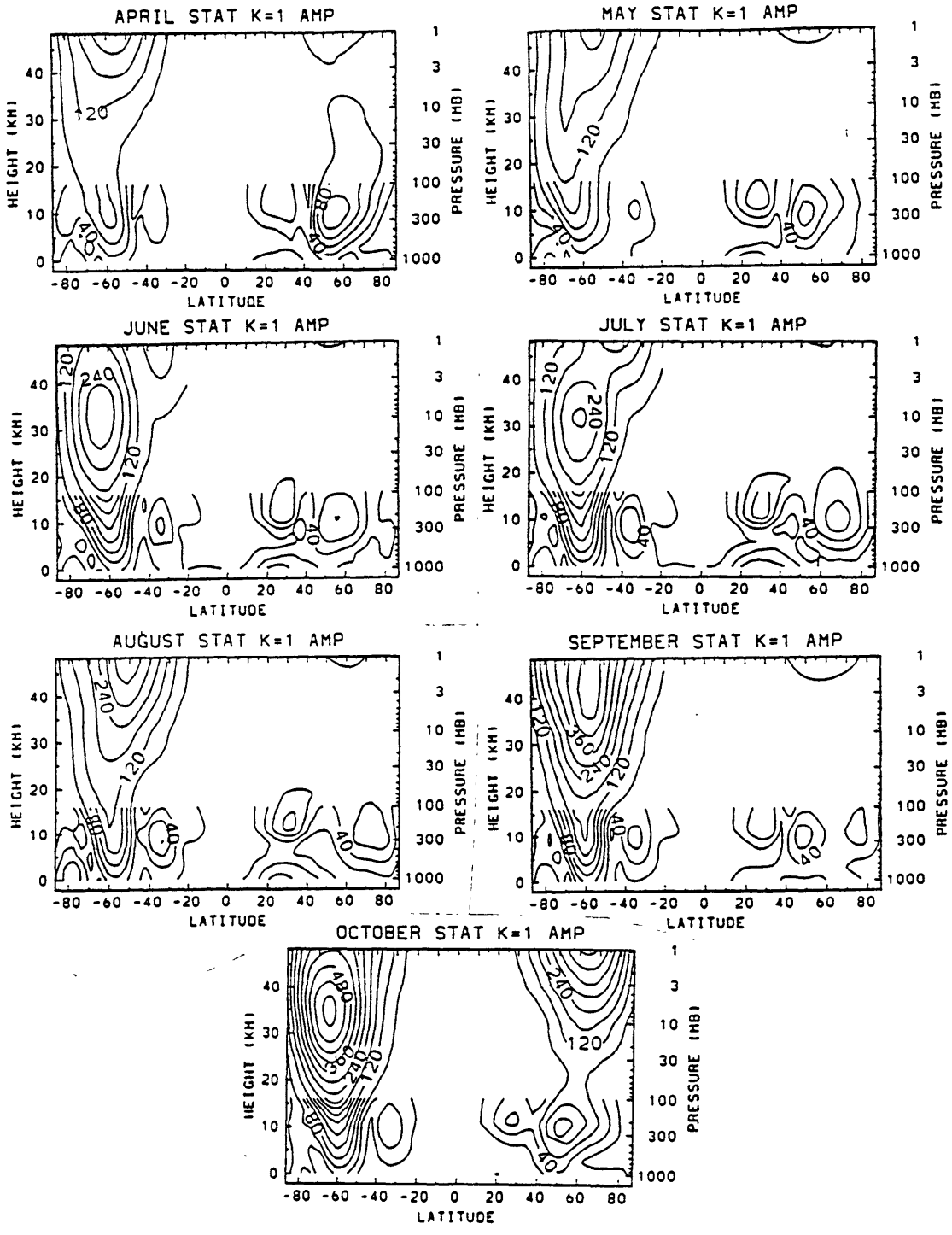

Figure 2.4: Stationary wave number 1 amplitude (in geop. m) for consecutive months. Contour interval: 60 m above 100 mb, 20 m below 100 mb. Meridional section. Figure from Randel (1987a).

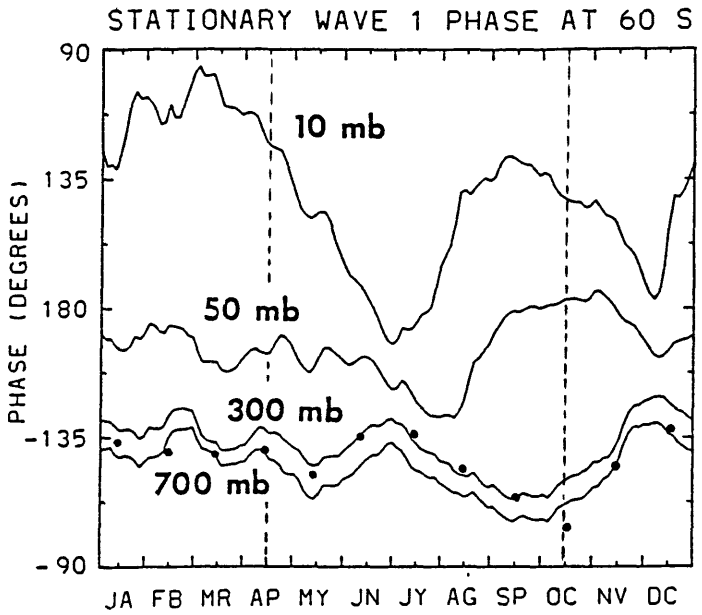

Figure 2.5: Seasonality in phase (longitude of crest, in degrees) of stationary wave 1 at 60°S for various pressure levels. The two vertical dashed lines delimit the months under consideration in the present study. The dots indicate monthly mean 300 mb data from Australian climatology. Figure from Randel (1988).

Chapter 3

The model

To address the questions raised in the introduction, a linear, stationary, quasi-geostrophic model on a hemisphere is considered. The flow is linearized about a purely zonal basic state flow. Forcing for the wave is introduced by specifying the wave at the lower boundary. In addition further boundary conditions and damping have to be prescribed. The following sketch schematically indicates the model's "action":

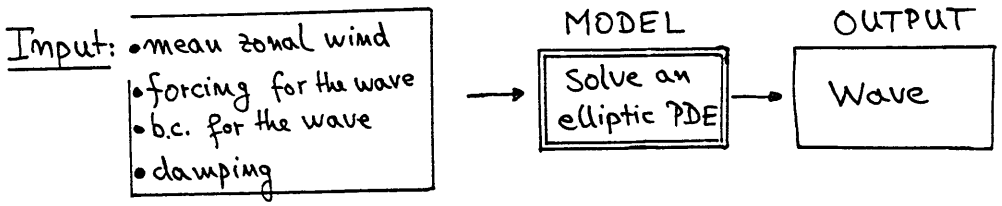

The present chapter describes the model equations, the applied boundary conditions, the form of damping used, and the numerical implementation of the model.

Stationarity is a reasonable approximation to the extent that the basic state varies slowly as compared with the time required to establish a stationary wave. In order to model the seasonal behaviour of the Southern Hemisphere winter, we consider monthly mean basic states for subsequent months, ranging from April through October. The model's basic state, therefore, changes on a timescale of a season. On the other hand, the vertical group velocity for

propagationg planetary waves is of the order of a few kilometers per day (see e.g. Karoly and Hoskins, 1982). Thus the wave should be able to reach a steady state on a much shorter timescale than a season, and hence the interseasonal change of the basic state can be considered to be "quasi- static" with respect to the wave propagation.

Interannual variability is of some concern to the present model. Since the wave (i.e. the calculated response of the model) depends nonlinearly on the zonal wind field, the use of climatological means from observations is only valid to the extent that there is little interannual variability.

Not all of the model assumptions can be regarded as good approximations to reality. After all, we do not contend to precisely simulate all the relevant physics with our simple model. We rather want to investigate, if and to what extent essential features of the wave propagation and of its seasonal cycle, as presented in the previous chapter, can be reproduced qualitatively. In particular we want to examine if the interpretation of the midwinter minimum suggested by A. Plumb's simple model (Plumb, 1989a, see introduction) carries over to the present, more detailed model, and we want to study to what extent the seasonal cycle of the wave can be related to the behaviour of the refractive index. Some of the model assumptions will be justified later in chapter 5, where we will show the robustness of the model with respect to those assumptions.

3.1 Model equations

As for quasigeostrophic theory on a hemisphere, we essentially follow Matsuno (1970). Beyond the usual assumptions for quasigeostrophic theory on a beta plane (see e.g. Andrews et al., 1987), on a hemisphere one has to require in addition

$$L \ll a \,, \tag{3.1}$$

where L is the horizontal scale of the motion in meridional direction, and $a = 6370$ km is the radius of the earth. This assumption is not a very good approximation when applied to the waves under consideration, since they have almost global extent (see figure 2.4).

Quasigeostrophic theory is invalid near the equator. In our case this

is not a severe limitation, since the basic state wind profiles for all months considered yield strong wave absorption in the tropics (see below, section 3.3). Therefore one does not expect noticable influence from the equatorial region or from beyond. On the other hand, in order to simulate the transmision characteristics of the atmosphere for waves qualitatively correctly, it is essential to use spherical geometry and to allow for both vertical and meridional propagation (Karoly and Hoskins, 1982).

Starting point in quasigeostrophic theory is the quasigeostrophic potential vorticity equation. Assuming small amplitude waves, this equation is linearized about a zonal basic state flow $\bar{u}$. For $\bar{u}$ we use the zonal component of the monthly mean zonal mean wind from Randel (1987a), as presented in chapter 2. As for the notation, an overbar signifies a basic state quantity and a prime stands for a perturbation quantity. Spherical coordinates are used, with λ denoting longitude and φ latitude (where values of φ are negative in the Southern Hemisphere). Altitude is measured in log-pressure coordinates

$$z \equiv -H \ln\left(\frac{p}{p_0}\right) , \tag{3.2}$$

with the scaleheight H chosen to be $H = 7$ km and the reference pressure p_0 chosen to be $p_0 = 200$ mb.[1] For use in our plots we introduce a second log-pressure coordinate

$$\hat{z} \equiv -H \ln\left(\frac{p}{1000 \text{ mb}}\right) , \tag{3.3}$$

which gives approximately the altitude above the earth's surface.

In these (λ, φ, z)-coordinates the stationary, linearized quasigeostrophic potential vorticity equation, modified to include the small advection of planetary vorticity by the ageostrophic wind,[2] is given by

$$\bar{\omega}\frac{\partial q'}{\partial \lambda} + \frac{v'}{a}\frac{\partial \bar{Q}}{\partial \varphi} = \mathcal{H}' , \tag{3.4}$$

where

$$\bar{\omega}(\varphi, z) = \frac{\bar{u}(\varphi, z)}{a \cos\varphi} \tag{3.5}$$

[1] $p_0 = 200$ mb is the lower boundary of the domain considered in our model.

[2] For a detailed derivation of the equation see Plumb (1989b).

is the angular velocity of the mean flow, and

$$\frac{1}{a}\frac{\partial \bar{Q}}{\partial \varphi} = \frac{2\Omega \cos\varphi}{a} - \hat{\Delta}\bar{u} \tag{3.6}$$

is the basic state quasigeostrophic potential vorticity gradient, with $\Omega = 7.292 \times 10^{-5}$ sec^{-1} denoting the angular velocity of the rotating earth. The zonal (u') and meridional (v') perturbation geostrophic velocities

$$u' = -\frac{1}{a}\frac{\partial \psi'}{\partial \varphi} \tag{3.7}$$

$$v' = \frac{1}{a\cos\varphi}\frac{\partial \psi'}{\partial \lambda} \tag{3.8}$$

and the perturbation quasigeostrophic potential vorticity

$$q' = \hat{\Delta}\psi' \tag{3.9}$$

are given in terms of the perturbation streamfunction ψ', which is related to the perturbation geopotential Φ' as follows:

$$\psi'(\lambda, \varphi, z) = \frac{\Phi'(\lambda, \varphi, z)}{2\Omega \sin\varphi} \, . \tag{3.10}$$

The Laplace-like operator $\hat{\Delta}$ is of the following form:

$$\hat{\Delta} \equiv \frac{1}{(a\cos\varphi)^2}\frac{\partial^2}{\partial \lambda^2} + \frac{\tan\varphi}{a^2}\frac{\partial}{\partial \varphi}(\cot\varphi \frac{\partial}{\partial \varphi}) + \frac{4\Omega^2 \sin^2\varphi}{p}\frac{\partial}{\partial z}\left(\frac{p}{N^2}\frac{\partial}{\partial z}\right) . \tag{3.11}$$

The buoyancy frequency squared $N^2(\varphi, z)$ is calculated from the basic state temperature $\bar{T}(\varphi, z)$ according to

$$N^2 \equiv \frac{R}{H}\left(\frac{\partial \bar{T}}{\partial z} + \frac{\kappa}{H}\bar{T}\right) , \tag{3.12}$$

with $\kappa \equiv R/c_p = 2/7$, the gas constant for dry air $R = 287$ J/(kg K), and c_p denoting the specific heat at constant pressure. Data for the basic state temperature $\bar{T}(\varphi, z)$ are, again, taken from Randel (1987a).

The nonconservative term $\mathcal{H}'$, containing friction ($\mathcal{F}'_\lambda, \mathcal{F}'_\varphi$) and diabatic heating $\mathcal{Q}'$, is given by

$$\mathcal{H}' = \frac{1}{a\cos\varphi}\left[\frac{\partial \mathcal{F}'_\varphi}{\partial \lambda} - \sin\varphi\frac{\partial}{\partial \varphi}(\mathcal{F}'_\lambda \cot\varphi)\right] + \frac{2\Omega\sin\varphi}{p}\frac{\partial}{\partial z}\left(p\frac{R\mathcal{Q}'}{HN^2}\right) . \tag{3.13}$$

Assuming Rayleigh friction and Newtonian cooling with equal coefficients α

$$(\mathcal{F}'_\lambda, \mathcal{F}'_\varphi) = -\alpha(u', v') \tag{3.14}$$

$$\mathcal{Q}' = -\alpha T' \tag{3.15}$$

reduces $\mathcal{H}'$ to

$$\mathcal{H}' = -\alpha q' \,. \tag{3.16}$$

The solution for ψ' is Fourier decomposed in zonal direction. In other words, we specifically look for solutions of the form $\psi' = \Re\, F(\varphi, z)\exp(is\lambda)$, where s is the zonal wave number, $F(\varphi, z)$ is some (complex) function, and $\Re$ ... denotes the real part of all that follows to its right. Moreover we restrict ourselves to *zonal wave number 1* in our whole study, since the very low wave numbers dominate the stationary wave field in the stratosphere (Randel, 1988). The reason therefore is because primarily waves of low wave numbers are forced in the troposphere, and moreover only the lowest wave numbers can substantially propagate upward into the stratosphere.

Using the following Ansatz for the perturbation stream function

$$\psi'(\lambda, \varphi, z) = \Re\, N(\varphi, z)\Psi(\varphi, z)\exp(\frac{z}{2H})\exp(is\lambda)\,, \tag{3.17}$$

the equation 3.4 reduces (after some amount of algebra) for the special case of $\mathcal{H}' = 0$ to an equation for $\Psi(\varphi, z)$:

$$\boxed{\otimes\Psi(\varphi, z) + \nu_s\Psi(\varphi, z) = 0} \tag{3.18}$$

where

$$\otimes \equiv \tan\varphi\frac{\partial}{\partial\varphi}(\cot\varphi\frac{\partial}{\partial\varphi}\ ) + \left(\frac{2\Omega a}{N}\right)^2 \sin^2\varphi\frac{\partial^2}{\partial z^2} \tag{3.19}$$

and

$$\nu_s = \frac{1}{\bar{\omega}\cos\varphi}\frac{\partial\bar{Q}}{\partial\varphi} - \frac{s^2}{\cos^2\varphi} - \frac{\varepsilon^2 a^2}{4H^2} - \varepsilon a^2\frac{\partial^2\varepsilon}{\partial z^2} + \frac{\varepsilon a^2}{H}\frac{\partial\varepsilon}{\partial z}\,, \tag{3.20}$$

with $\varepsilon = 2\Omega\sin\varphi/N$.

Equation 3.18 is the basic model equation. For a specified basic state and a certain zonal wave number s, the equation yields the wave structure of the linear, stationary wave in the meridional plane. Due to a formal analogy to geometric optics, the quantity ν_s is called *refractive index square.* Note that ν_s as defined here is a dimensionless quantity. In the following we will somewhat

loosely (but without the danger of confusion) refer to ν_s as the "refractive index". For a given s, the refractive index contains only information about the basic state and might therefore be useful as a diagnostic quantity. In fact, it was shown by Karoly and Hoskins (1982) that, qualitatively at least, the WKB method seems to work, and "ray paths" of wave activity are refracted toward larger values of the refractive index. More about the refractive index and its interpretation in our model will be presented in chapter 4.3.

The refractive index, and hence the whole equation 3.18, is singular along the so-called *critical lines*, i.e. where the basic state angular velocity $\bar{\omega}$ vanishes.[3] This is a characteristic feature of linear theory. Following Matsuno (1970) we formally avoid this singularity by inclusion of damping, which has to be taken into account anyway. To include the nonconservative term $\mathcal{H}'$ in equation 3.18, using equation 3.16, one has to substitute

$$\bar{\omega} \longrightarrow \bar{\omega} - \frac{i\alpha}{s} \tag{3.21}$$

in expression 3.20 for the refractive index. Thus dissipation makes the refractive index complex and therefore prevents the singularity of ν_s at critical lines. What really happens at a critical level is not entirely clear (see Andrews et al., 1987, and references therein, in particular Killworth and McIntyre, 1985). The assumption we make implicitly in our present treatment is that critical levels entirely absorb all incoming wave activity. With this approach the model can certainly not account for any reflection off the critical lines. To the extent that there is substantial reflection in nature, one may expect the model to fail.

3.2 Boundary conditions and forcing

In order to obtain a solution for equation 3.18, boundary conditions for $\Psi(\varphi, z)$ must be specified. Dirichlet boundary conditions are applied on all boundaries. In particular we model the wave forcing by imposing an inhomogeneous lower boundary condition. Figure 3.1 sketches the domain and its boundaries, for which the equation is solved. In latitude, we cover the area between the south pole ($-90°$) and $-10°$. The area of interest reaches from 200 mb (which corresponds to z = 0 km in our log-pressure coordinates) up to 1 mb (corresponding

[3]This is true for stationary waves. For waves with nonzero phase velocity, the critical line is defined to be the line where the basic state wind speed equals the wave's phase speed.

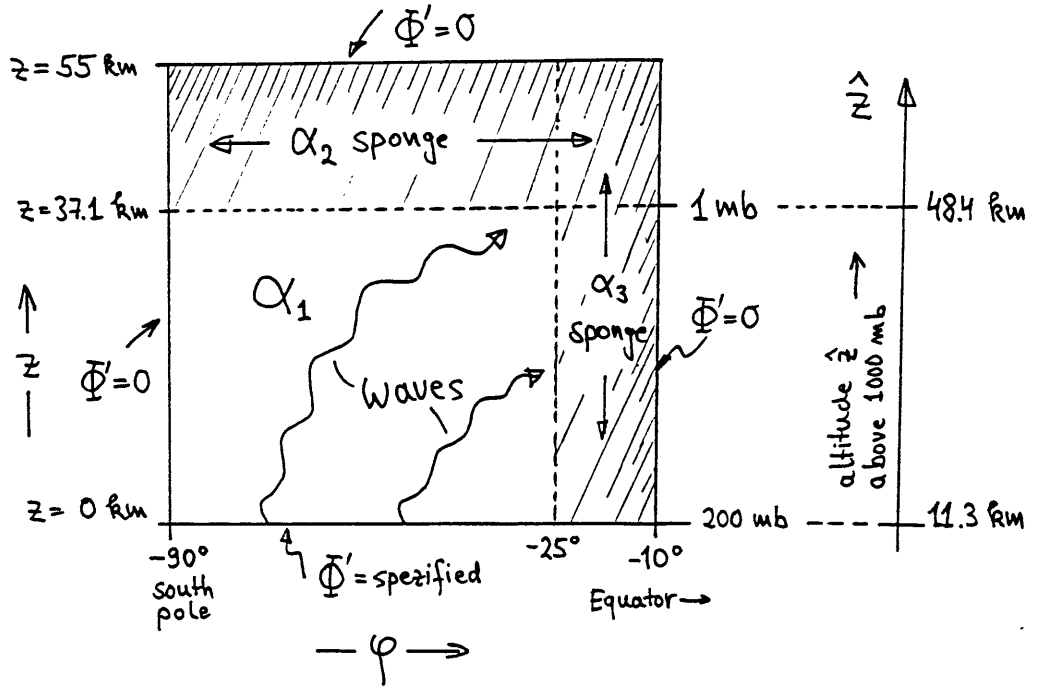

Figure 3.1: Sketch of the model domain in the meridional plane with the applied damping and boundary conditions.

to z = 37.1 km). Thus, in altitude we roughly contain what is usually referred to as the stratosphere. For technical reasons (see below), the computational domain is extended up to z = 55 km in altitude. If in the following we speak of a "meridional structure" or "meridional section", we mean a structure or a cross section in the meridional (φ, z)–plane. As opposed to this, "latitudinal" refers purely to the direction in latitude.

First we consider the lower boundary. Since the present study investigates transmission characteristics of waves rather than their generation mechanisms, forcing of middle atmospheric waves is modeled by simply specifying the stream function at the lower boundary, which was chosen to be the 200 mb level. This should be a reasonable approximation, since both major sources for planetary waves (orographic forcing and thermal forcing, see e.g. Held, 1983) are concentrated in the lower or middle troposphere, and thus the 200 mb level is above all major mechanisms for wave excitation. Monthly mean values for the stationary wave (s = 1) geopotential at 200 mb are taken from Randel (1987a). Figure 3.2 shows the time series of the climatological monthly mean

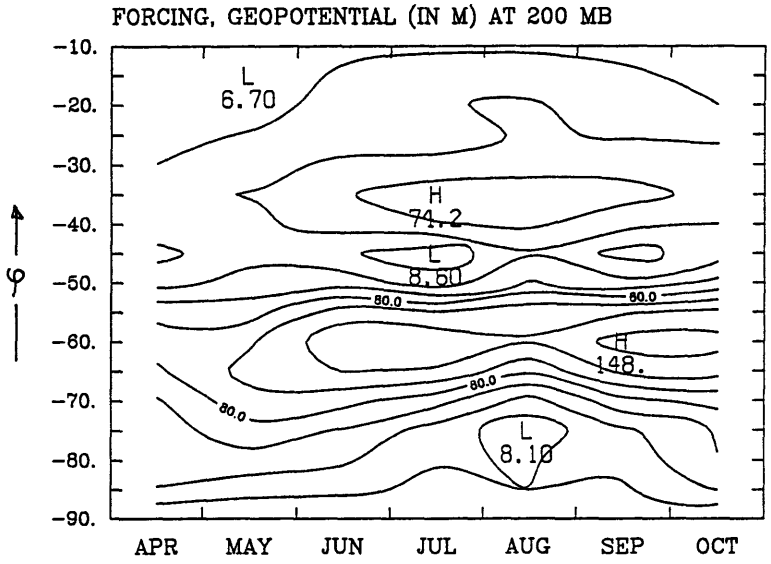

Figure 3.2: Seasonal cycle (latitude-time section) of the forcing: stationary wave 1 amplitude (geopotential, in geop. m) in the Southern Hemisphere at 200 mb. Data from Randel (1987a).

amplitude from April through October.

In order to obtain a single-valued streamfunction at the south pole, the boundary condition there is

$$\Psi(-90°, z) = 0 \,. \tag{3.22}$$

Since the overall direction of propagation of the waves is upward and equatorward, for the upper and equatorward boundary some radiation condition would seem to be the best choice. In order to circumvent related technical difficulties, however, we approach these two boundaries using the idea of a sponge layer. For this reason, the domain is extended by more than 15 km in altitude beyond the 1 mb level. In this additional layer, strong damping (see section 3.3) is applied in order to make the wave die down. Consequently, the stream function can be set to zero at the upper boundary of the computational domain $z_{\text{top}} = 55$ km:

$$\Psi(\varphi, 55 \text{ km}) = 0 \,. \tag{3.23}$$

The equatorward boundary is treated in a similar way, and the corresponding

boudary condition at the equatorward boundary $\varphi_{\text{bry}} = -10°$ is analogously:

$$\Psi(-10°, z) = 0 \,. \tag{3.24}$$

3.3 Damping

The damping coefficient α (equations 3.14 and 3.15) is chosen to be, equally for all months, the sum of three parts:

$$\alpha(\varphi, z) = \alpha_1(z) + \alpha_2(z) + \alpha_3(\varphi) \,. \tag{3.25}$$

The first part α_1 is supposed to model the real dissipation of the waves in the atmosphere, whereas the second and third part (α_2 and α_3) represent the damping contributions for the two sponge areas (see figure 3.1).

Guided by estimates for the Newtonian cooling coefficient (see Leovy, 1984, his figure 3), the physical part α_1 is chosen to be piecewise linear in the following way:

$$\alpha_1(z) = \begin{cases} 0.05 \text{ day}^{-1}, & z \leq 10 \text{ km} \\ \left(0.05 + \frac{z - 10 \text{ km}}{30 \text{ km}} 0.15\right) \text{ day}^{-1} & 10 \text{ km} < z \leq 40 \text{ km} \\ 0.2 \text{ day}^{-1}, & z > 40 \text{ km} \end{cases} \tag{3.26}$$

As for the sponge layers, the applied damping has to satisfy two requirements. On the one hand, the damping has to be strong enough, such that the wave dies out untill it reaches the boundary, where zero Dirichlet boundary condition is imposed. On the other hand, the increase in damping has to be slowly varying in space, since otherwise reflection will occur. The following choices for α_2 and α_3 prove to satisfy these requirements approximately:[4]

$$\alpha_2(z) = \exp\left(\frac{z - 50 \text{ km}}{3 \text{ km}}\right) \text{ day}^{-1} \,, \tag{3.27}$$

$$\alpha_3(\varphi) = \exp\left(\frac{\varphi + 15°}{3°}\right) \text{ day}^{-1} \,. \tag{3.28}$$

Figure 3.3 shows the total damping coefficient α. The contribution of the sponges α_2 and α_3 are negligible below 40 km and poleward of 25°, which is

[4] in the sense that considerably changing the shape and strength of α_2 and α_3 hardly affects the result

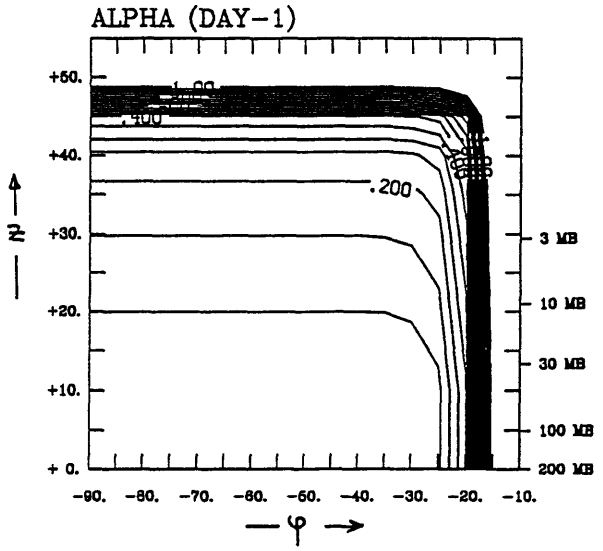

Figure 3.3: Damping coefficient α in day^{-1}. Contour interval is 0.05 day^{-1}; contours beyond 1 day^{-1} are not drawn. Meridional section. z in km, latitude in degrees.

the area of interest in this study. Besides being a technical trick, both sponges represent to some extent physically existing damping mechanisms: Planetary waves are being dissipated in the higher stratosphere due to nonlinear wave breaking mechanisms (McIntyre and Palmer, 1983), and critical lines[5] are assumed to act like a wave absorber (see above, end of section 3.1).

3.4 Numerical implementation

Equation 3.18 is two-dimensional elliptic partial differential equation. For its numerical solution on the domain shown in figure 3.1, the equation is discretized on a 17 by 12 point grid (latitude by altitude) with a gridspacing of 5° in latitude and 5 km in altitude. To solve the corresponding finite difference equation system, a direct solver (based on Lindzen and Kuo, 1969) is used.

The dependence of the model results on the numerical resolution was checked by increasing the number of grid points, i.e decreasing the grid-spacing.

[5]Note that in all months under consideration there is a critical line close to the equatorward boundary.

For instance, doubling the vertical resolution (using a 17 by 23 point grid) gives qualitatively precisely the same wave amplitude behaviour. Quantitatively the differences compared with the 17 by 12 grid are less than 2.5 %.

In order to assimilate the data from Randels (1987a) grid to the grid used in the present calculations, bicubic spline interpolation (Press et al., 1986) is used. Randel gives no data beyond 1 mb. Therefore the fields are extended above 1 mb by substituting the respective values from the 1 mb level.

Chapter 4

Model results and interpretation

In this chapter we present the results of the numerical implementation of our model. The calculated wave and related quantities will be compared with the observations from chapter 2, the influence of the forcing will be studied, and the model will be tested for internal consistency. Questions pertaining to the sensitivity of the model with respect to various parameters are deferred to chapter 5.

4.1 Basic state, wave and related diagnostics

To facilitate the comparison with subsequent plots, we show here in figure 4.1 again the basic state *zonal wind* $\bar{u}$ for the seven months under consideration. The data for this figure are identical with those from figure 2.2, but restricted to our domain of interest now. The labelling of the axes for this and all further plots of this kind is according to the following convention: The x-axis denotes latitude φ in degrees with the south pole on the left hand side, and the y-axis denotes altitude in three different units, namely as z (equation 3.2) in km, $\hat{z}$ (equation 3.3) in km and pressure in mb.

Figure 4.2 gives the basic state *potential vorticity gradient* $\partial\bar{Q}/\partial(a\varphi)$ as calculated according to equation 3.6. The strong westerly polar night jet manifests itself through its curvature as high positive values in $\partial\bar{Q}/\partial(a\varphi)$. As

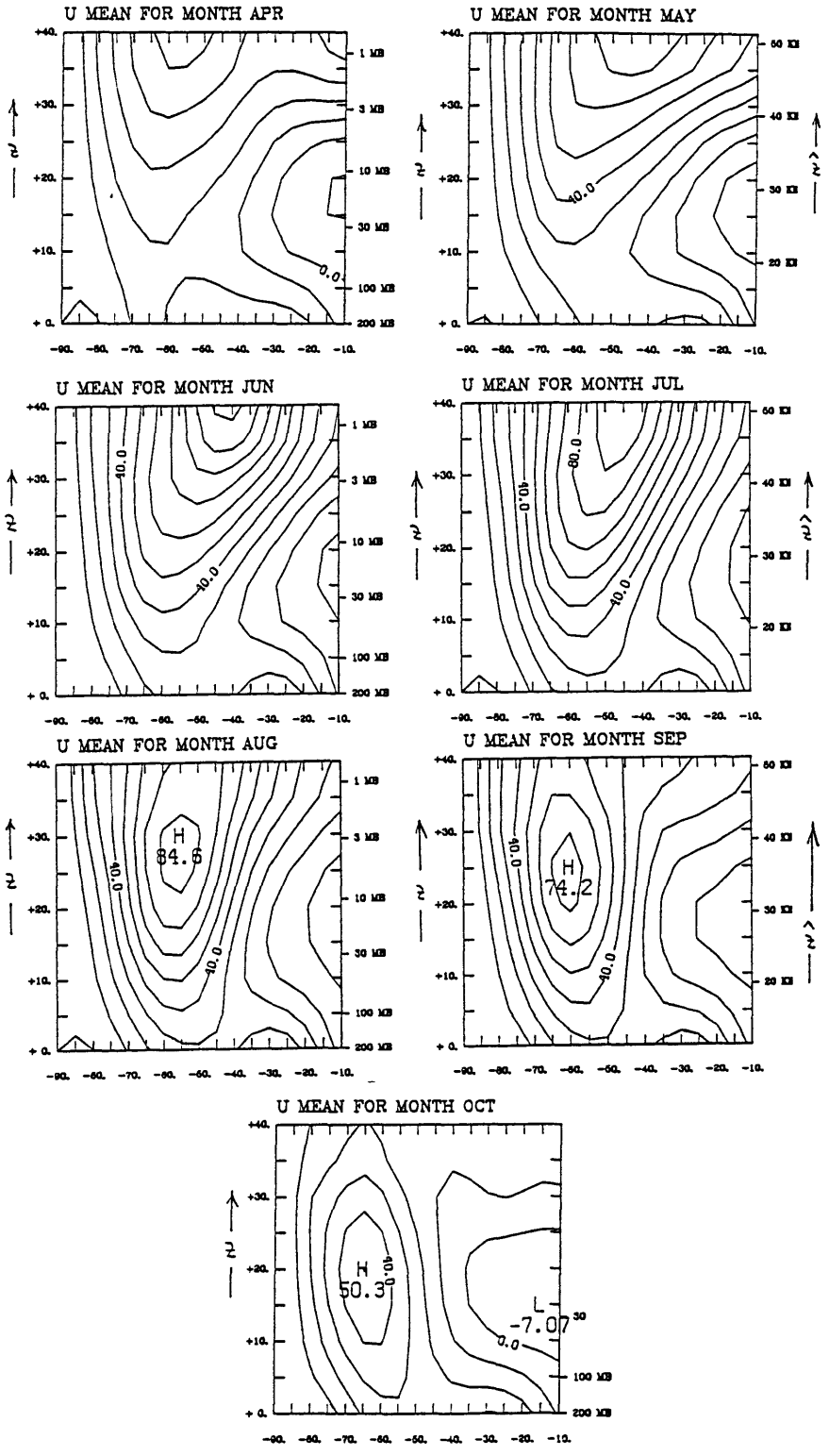

Figure 4.1: Basic state zonal wind (in m/sec) for subsequent months. Contour interval: 10 m/sec. Meridional section. z and $\hat{z}$ in km, latitude in degrees. Data from Randel (1987a).

opposed to the idealized basic state wind fields used by Matsuno (1970) or Schoeberl and Geller (1977), our present wind fields are such that $\partial\bar{Q}/\partial(a\varphi)$ is *not* positive everywhere; it rather changes sign within the domain and has negative values close to the pole.

The *refractive index* ν_s for $s = 1$ as derived from the basic state wind according to equation 3.20 is shown in figure 4.3. The overall features of ν_s are similar for all months: high values near the equator, low and negative values (note that no negative contours are ploted) near the pole, a local minimum in midlatitudes close to the lower boundary, and a ridge like feature in higher latitudes (between about $-55°$ and $-70°$) extending into the middle stratosphere. Randel (1988) points out that the substantial variation of $\bar{u}$ and $\partial\bar{Q}/\partial(a\varphi)$ during the period is not reflected in a corresponding variation of the refractive index. For instance, the magnitude of the high latitude ridge is around 25 to 35 for all months. This comes essentially from the structure of the expression for ν_s, which includes a division of $\partial\bar{Q}/\partial(a\varphi)$ by $\bar{u}$ (see equation 3.20). However, a somewhat closer look reveals certain differences between the single months. The magnitude of the refractive index close to the lower boundary changes considerably, as does the exact location of the midlatitude low altitude minimum. In April, for instance, the high latitude ridge reaches a maximum value of only around 13 at the 100 mb level and the local low level minimum lies at about $-56°$, while in August the ridge reaches a maximum value of over 30 at the 100 mb level and the minimum lies at about $-38°$. To the degree that these more detailed structures are real, they might turn out to be significant in the interpretation of this diagnostic (see section 4.3). On the other hand we want to note that the smallest scale structures of the potential vorticity gradient and refractive index should not be taken too seriously, since their calculation involves second derivatives of data, which leads to amplification of small scale noise.

We concentrate in our study on the stationary wave 1. Decomposing the corresponding perturbation geopotential according to

$$\Phi'(\lambda, \varphi, z) = \Re \; A \exp(i\Theta) \exp(i\lambda) \tag{4.1}$$

we consider the real amplitude $A(\varphi, z)$ and phase $\Theta(\varphi, z)$ separately. First we show the *amplitude* $A(\varphi, z)$ in figure 4.4. Generally, it increases with altitude in the lower stratosphere. This is essentially due to the pressure decreasing with height: a merely vertically propagating, undamped wave in a constant

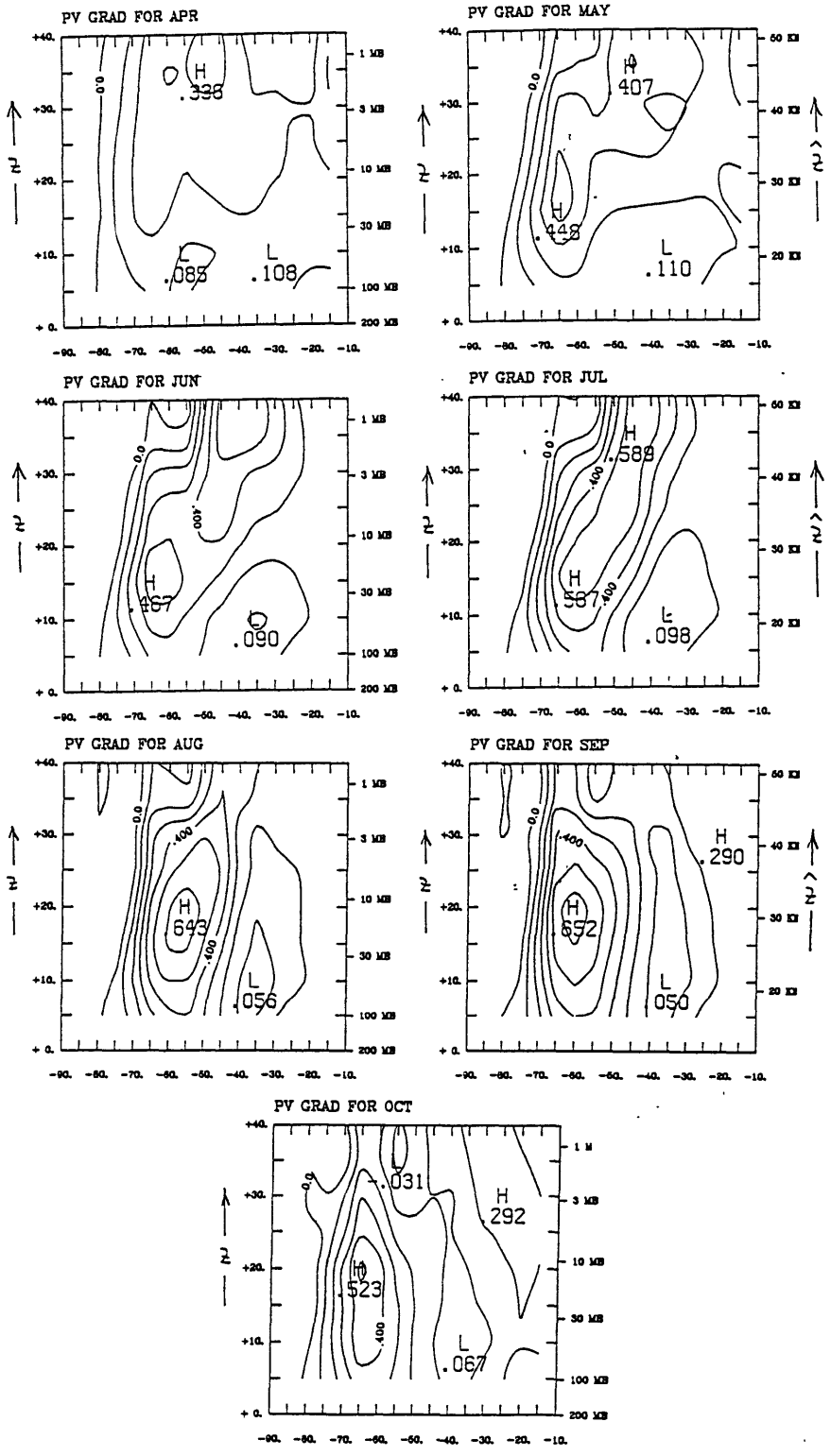

Figure 4.2: Basic state potential vorticity gradient (in $10^{-10}\mathrm{m}^{-1}\mathrm{sec}^{-1}$). Contour interval: $0.1 \times 10^{-10}\mathrm{m}^{-1}\mathrm{sec}^{-1}$. Only non-negative contours are drawn. Meridional section. z and $\hat{z}$ in km, latitude in degrees.

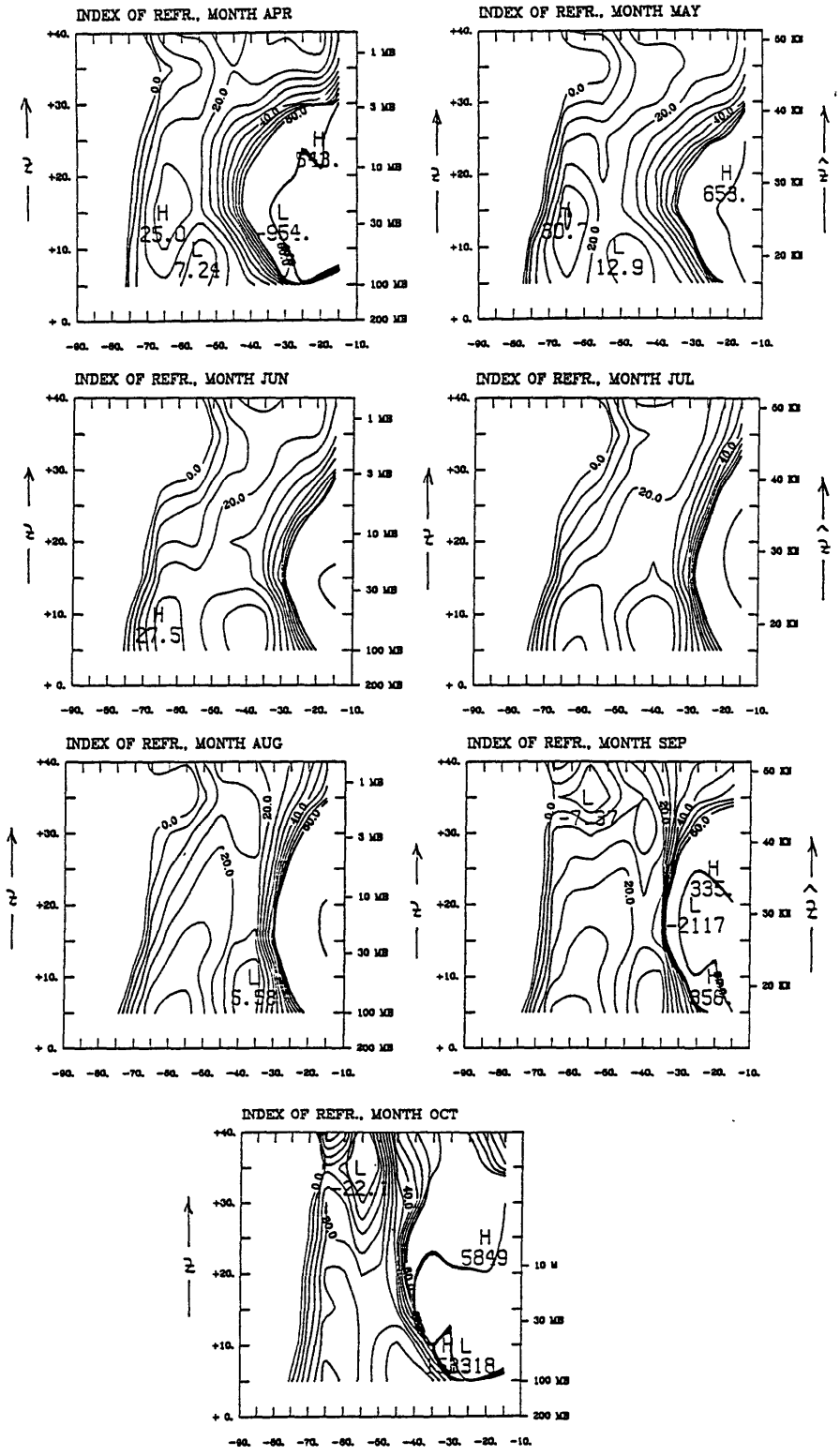

Figure 4.3: Refractive index ν_s for s=1. Contour interval: 5. No contours are plotted for values less than zero and larger than 60. Meridional section. z and $\hat{z}$ in km, latitude in degrees.

basic state flow would grow according to $\propto \exp[z/(2H)]$ (Charney and Drazin, 1961; see also below, section 4.3). Above about 50 mb the ridge of amplitude lies approximately along the maximum of the polar night jet for all months. In particular, in later months the location of the wind maximum and the wave maximum agree well. Note that this close relationship between the maximum of wave amplitude and that of the westerly maximum is consistent with the observations (see chapter 2).

As mentioned earlier, we do by no means try to simulate the atmosphere in a quantitative manner with our model. However, comparing the general behaviour of the calculated amplitude from figure 4.4 with the observations from figure 2.4 reveals even *qualitative differences* . The model does not reproduce the observed increase of amplitude with altitude in April and May, neither is the observed pronounced maximum around the 10 mb level in June and July captured. Above all, the model does *not* yield the characteristic seasonal cycle of wave amplitude in the higher stratosphere. Analogous to the plot with the observations (figure 2.3), figure 4.5 presents the seasonal cycle of the calculated amplitude for several different pressure levels. As opposed to the observations there is no evidence for a maximum in wave amplitude in early winter, neither is there a minimum in midwinter.

The dominating feature of the calculated wave's *phase* $\Theta(\varphi, z)$ (figure 4.6) is a westward tilt with height and westward tilt towards the equator. It indicates upward and equatorward wave activity propagation (see below), which is consistent with observations (see Randel, 1987a). However, a more detailed comparison of the model with observations reveals, again, discrepancies. Corresponding to figure 2.5 we show in figure 4.7 a time series of the calculated phase at three different pressure levels. The location of the ridge at 10 mb is considerably off the observed location, in the sense that the observed wave has stronger tilt with height than the calculated wave. Also, the difference in vertical phase tilt between early winter (June and July) and late winter (September and October) is not by far as pronounced as in the observations.

Finally we consider the *Eliassen-Palm* (EP) *flux* (F_φ, F_z), which has become a well-established diagnostic. Its direction indicates the direction of wave activity propagation, and its divergence gives information about wave mean flow interaction (see Andrews et al., 1987). Here we calculate the EP flux in quasigeostrophic approximation, which reduces for the present stationary

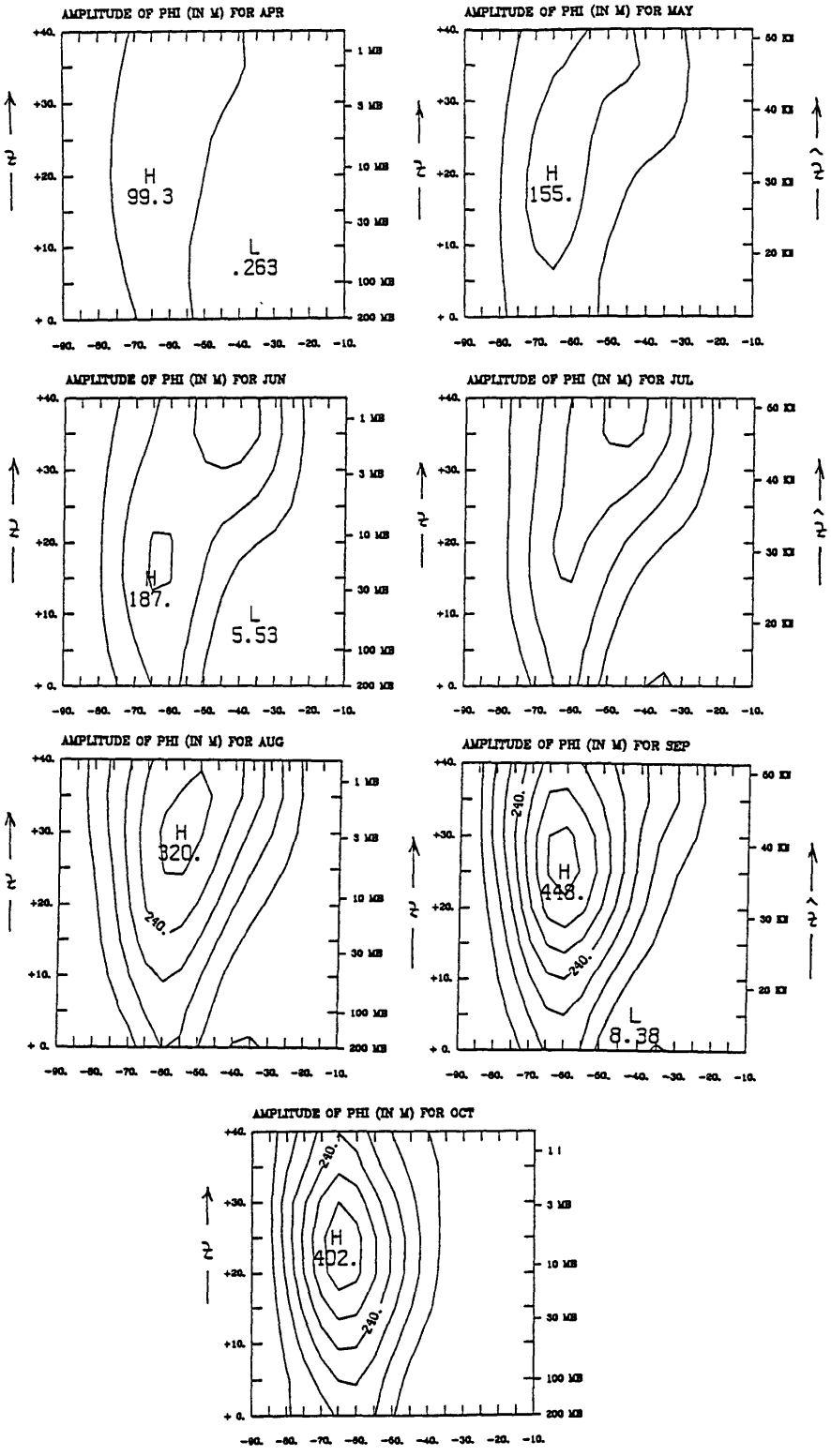

Figure 4.4: Calculated amplitude A (in geop. m) for subsequent months. Contour interval: 60 m. Meridional section. z and $\hat{z}$ in km, latitude in degrees.

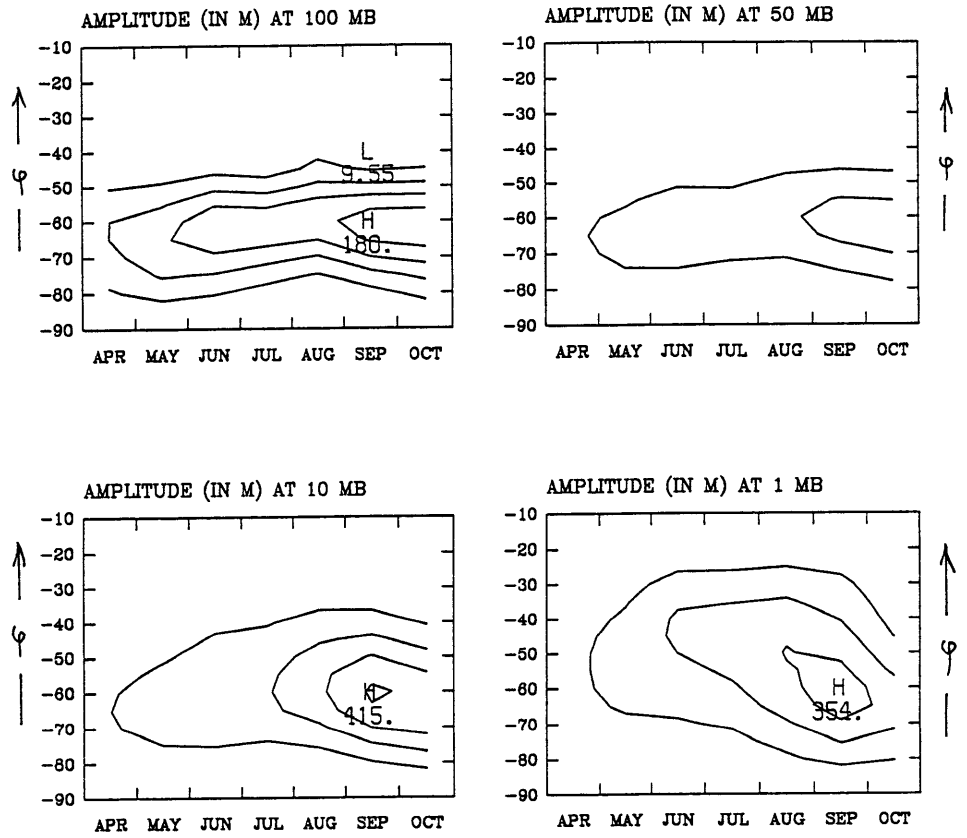

Figure 4.5: Calculated amplitude A (in geop. m) in a latitude-time plot at four different pressure levels. Contour interval: 40 m at 100 mb, 100 m otherwise.

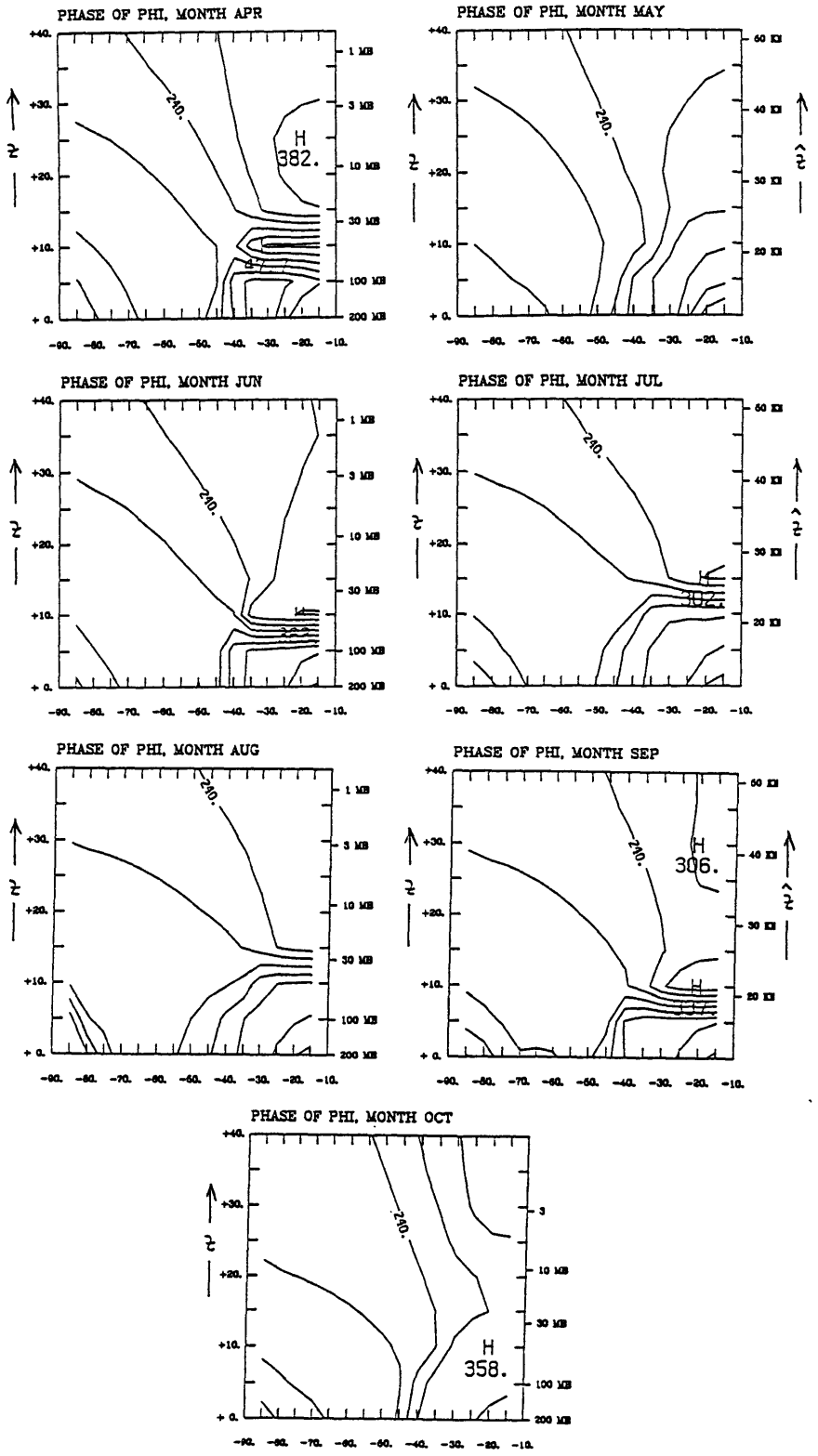

Figure 4.6: Calculated phase Θ (in degrees). Contour interval: 60°. Meridional section. z and $\hat{z}$ in km, latitude in degrees.

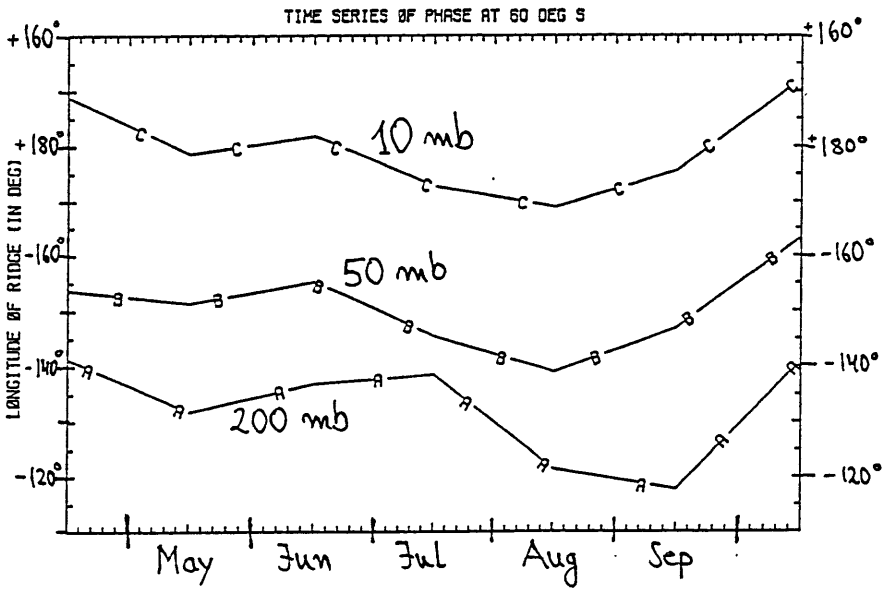

Figure 4.7: Calculated seasonality in phase (longitude of ridge, in degrees) at 60°S for three different pressure levels: 200 mb (curve A), 50 mb (curve B) and 10 mb (curve C).

wave 1 to:

$$F_\varphi = \frac{1}{2}\rho_0 \frac{A^2}{f^2}\frac{\partial\Theta}{\partial(a\varphi)} \tag{4.2}$$

$$F_z = \frac{1}{2}\rho_0 \frac{A^2}{N^2}\frac{\partial\Theta}{\partial z} \tag{4.3}$$

with the Coriolis parameter $f = 2\Omega\sin\varphi$ and the basic state density $\rho_0 = 1.0\exp(\hat{z}/H)$ kg/m^3. The EP flux depends on the wave amplitude square and the gradient of the phase. In figure 4.8 we present the *normalized* EP flux. The arrows are scaled such that they point in the *direction* of wave activity propagation.

The overall structure of the EP flux diagrams in the middle and upper stratosphere is quite similar for all months: it is dominated by upward and equatorward propagation. Even though the single months differ slightly in the direction of the EP flux (in particular in the lower stratosphere), the quite substantial differences in amplitude between different months (compare e.g. April and October) are not all too obviously reflected in corresponding differences in the direction of wave propagation. Major differences in the

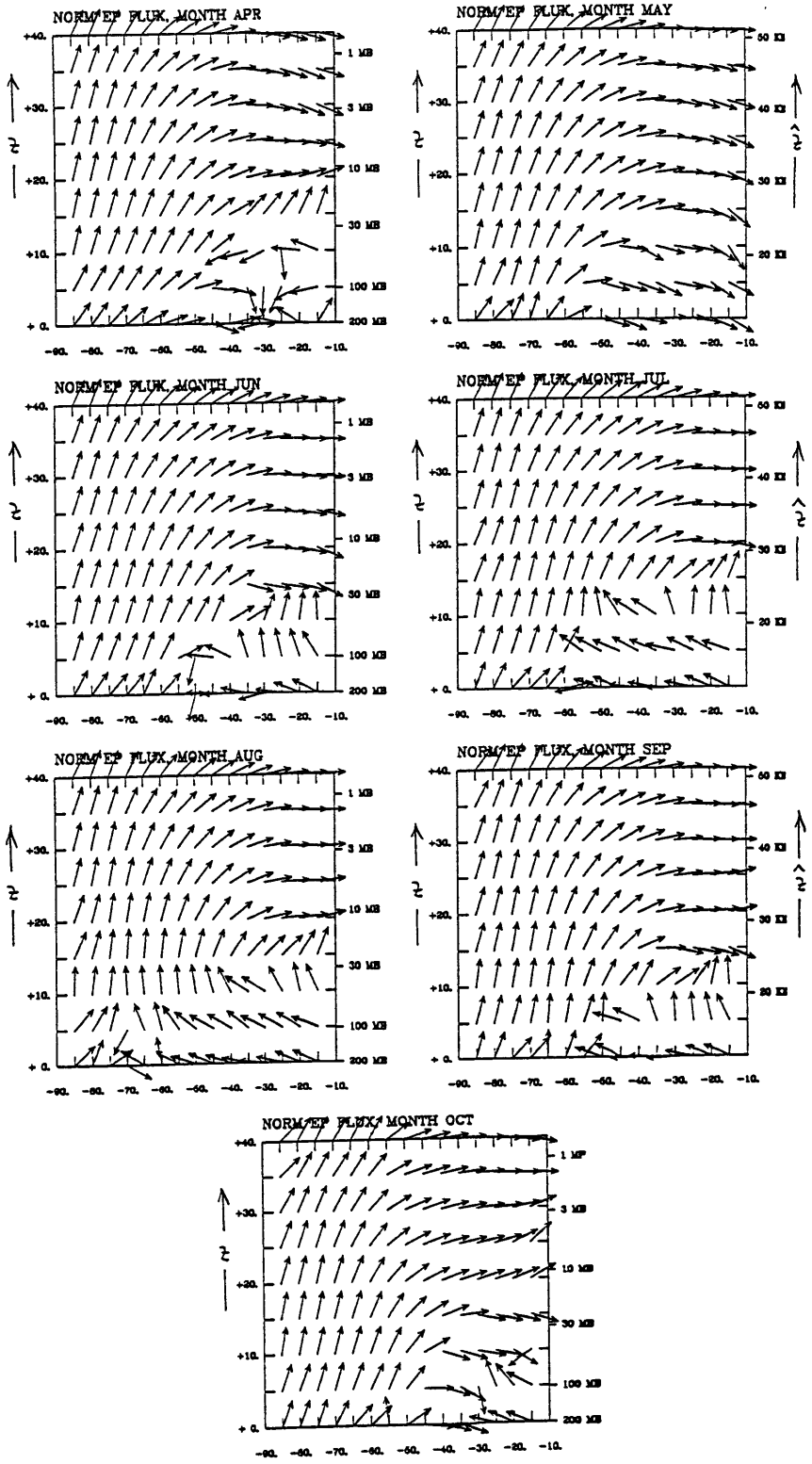

Figure 4.8: Calculated normalized EP flux. Meridional section. z and $\hat{z}$ in km, latitude in degrees.

wave amplitude seem to be accompanied by minor differences in the EP flux direction. Thus the use of the EP flux direction as a diagnostic, should it turn out to be usefull at all, would at least require a quite careful analysis.

The strong equatorward component of the EP flux emphasizes the importance of using a model which includes meridional wave propagation and which handles the processes occuring in the equatorial latitudes (critical lines!) reasonably well. The prevalent upward propagation is naturally to be expected, since the wave is forced from below. Equatorward propagation is consistent with the qualitative behaviour of the refractive index (higher values towards the equator) and its usual interpretation (ray paths are refracted towards higher values, see e.g. Karoly and Hoskins, 1982). However, Karoly and Hoskins (1982) point out that spherical geometry alone leads to an overall tendency for equatorward wave propagation. Hence, the refractive index is at best one part of the "explanation" for the overall direction of propagation.

The wave amplitude does not grow like $\propto \exp[z/(2H)]$, but shows instead weaker growth with height and even decreases with height in the higher stratosphere in some months, thus forming a maximum in the middle stratosphere. We refer to the location of this maximum as "vertical penetration" (cf. Simmons, 1974). It certainly depends on the amount of damping in the atmosphere. However, the direction of wave propagation contributes to the vertical penetration, too. For, in the model the wave gets strongly damped in equatorial latitudes and hence all wave activity that is directed towards the equator is "lost". Therefore growth with height must be weaker as compared with a model with purely vertical propagation. Yet, due to the overall similarity of the EP flux plots it seems impossible to infer from them, even qualitatively, the widely varying vertical penetration for the different months.

4.2 Impact of the forcing

The seasonal cycle of the wave in the upper stratosphere may arise either from variations in the forcing or from variations in the transmission characteristics of the atmosphere, or from both. In order to correctly estimate the influence of the basic state and its transmission properties alone, we investigate the impact of the seasonal cycle of the forcing in this section.

The observed wave amplitudes already give a strong indication that the main contribution comes from the variation in wave transmission rather than variation in forcing. While the amplitude maximum at the 200 mb level (our forcing level, see figure 3.2) varies from about 90 m in April to 150 m in October (roughly 60 % variation), the amplitude maximum at the 10 mb level (figure 2.3) varies from 120 m in April to over 600 m in October (a factor 5).

In a linear model the two effects (forcing and transmission) can be separated and their influence can be assessed independently. This is done in the following way. Instead of specifying the observed wave at 200 mb, we specify, equally for all months, constant wave amplitude and phase at the lower boundary according to:

$$A(\varphi, p = 200 \text{ mb}) = \begin{cases} 80 \text{ m} & \text{for } -85° \leq \varphi \leq -15° \\ 0 \text{ m} & \text{for } \varphi = -90° \text{ and } \varphi = -10° \end{cases}$$

$$\Theta(\varphi, p = 200 \text{ mb}) = 0° \quad \text{for } -90° \leq \varphi \leq -10°$$

In this "constant forcing" case all the resulting variation in the wave response must be due to variation in the basic state and its transmission characteristics. Figure 4.9 shows the result. The structure of the wave amplitudes in the middle and upper stratosphere is quite similar to the runs with realistic forcing (figure 4.4). Comparison of the response at 1 mb for the two cases (figure 4.10) shows that the characteristic seasonal cycle of the model response is virtually independent of the exact forcing.

The EP flux direction field for the case of constant forcing is shown in figure 4.11. The arrows start vertically off the lower boundary, since by specification there is no phase variation with latitude. Overall, the fields for the different months are even more similar to each other than in the case of realistic forcing. Hence, the quantitative and qualitative differences in wave amplitude from figure 4.9 can hardly be explained from the direction of the wave activity propagation.

In summary, essentially all qualitative and most quantitative differences between the single months can be attributed to variations in the basic state and its transmission properties. In other words, the comparatively weak seasonal cycle in forcing plays a minor role in determining the strong seasonal cycle of the model response.

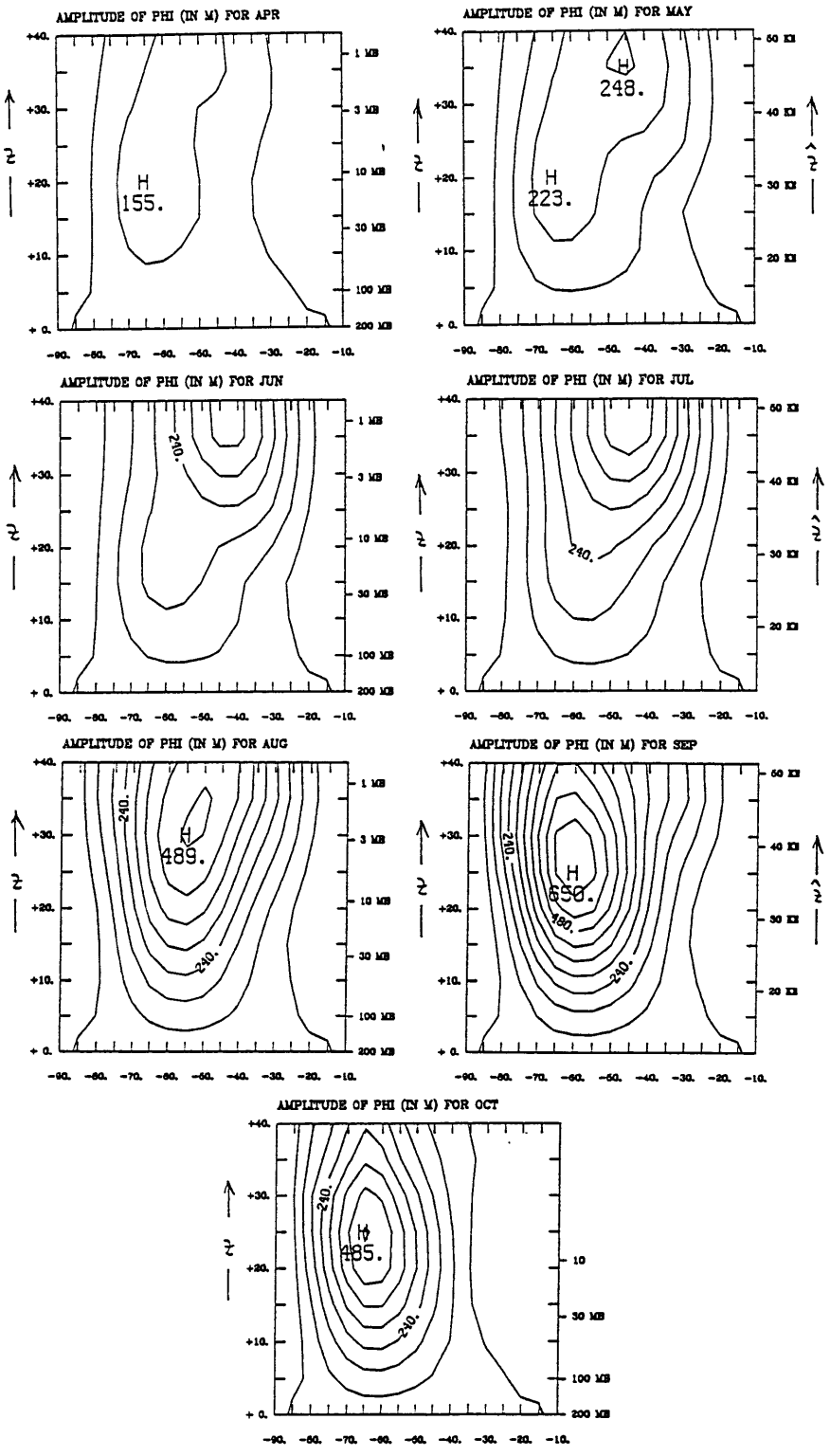

Figure 4.9: Model wave amplitude in meridional section as in figure 4.4, only constant forcing (80 m amplitude, zero phase) at the lower boundary.

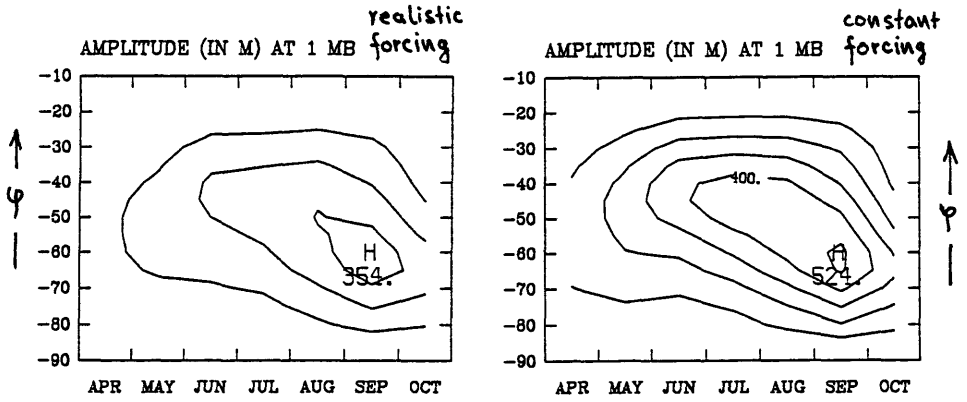

Figure 4.10: Seasonal cycle of the model wave amplitude (in geop. m) at 1 mb. Left panel: realistic forcing; right panel: constant forcing (80 m). Contour interval: 100 m.

4.3 Consistent interpretation

So far in this chapter we saw that the model reproduces the overall structure of the observed wave reasonably well. However, we found disagreement with observations in more detailed features, especially in the seasonal cycle. In this section we want to show that the model results are internally consistent: It is possible to rationalize the model's seasonal cycle (as opposed to the observed seasonal cycle) and the structure of the wave in the meridional plane through a specific interpretation of the basic state and its diagnostics. These interpretations are by no means far-fetched, but quite consistent with previous research about the refractive index and the overall behaviour of our model equation.

4.3.1 Seasonal cycle

First we relate the seasonal cycle of the wave (as displayed by the amplitude in the higher stratosphere, figure 4.5) to the seasonal behaviour of the refractive index. The usual interpretation of refractive index assumes WKB approximation. This means that the rate of change of the basic state is small over the distance of one wavelength of the solution. It can be shown (Andrews et al., 1987) that the WKB solution locally looks like a plane wave and that the equation 3.18 reduces to an equation analogous to the two-dimensional equation for a light wave in a medium of varying refractive index. Thus the "ray paths", along which wave activity propagates, are refracted towards higher

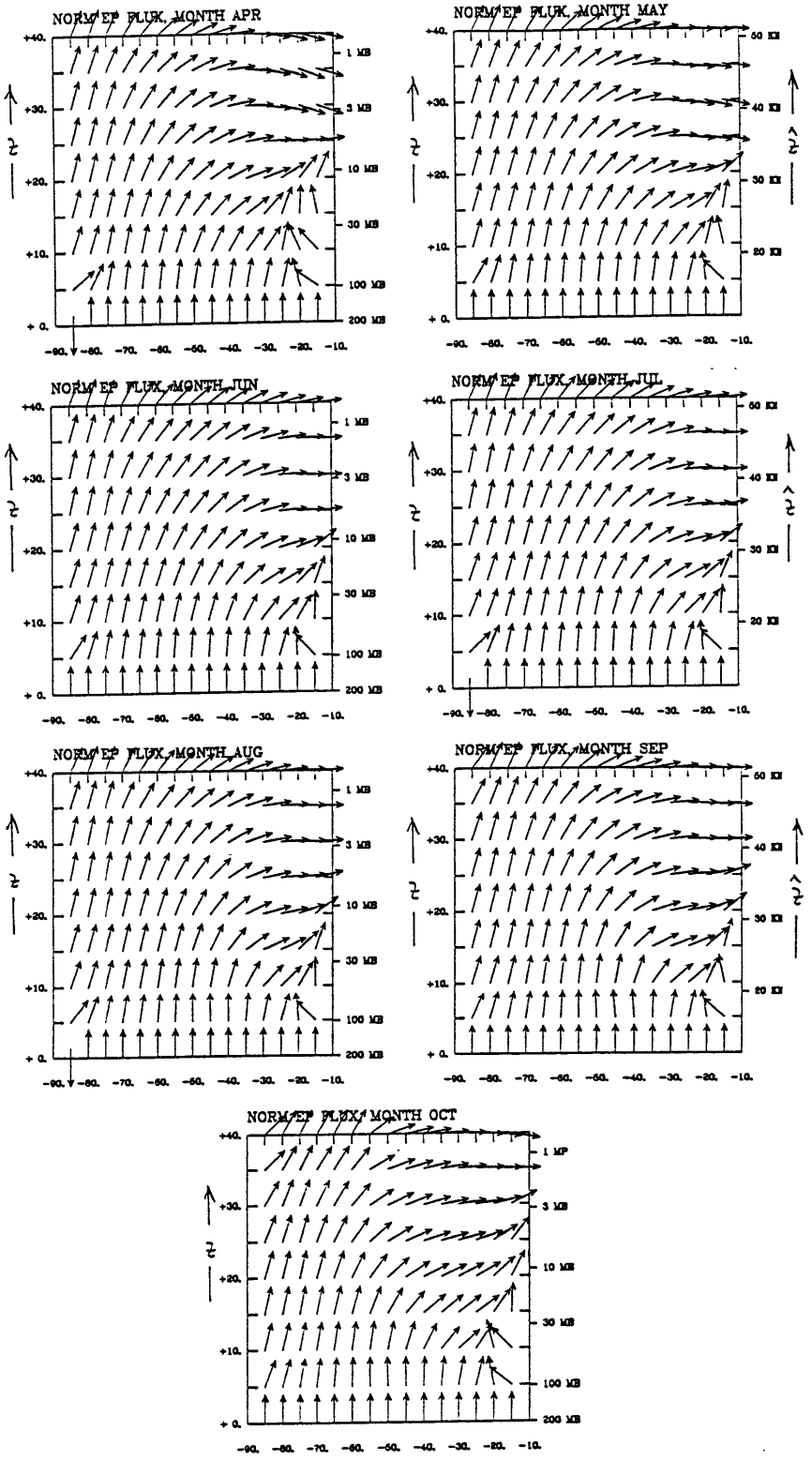

Figure 4.11: Normalized EP flux vectors as in figure 4.8, only constant forcing (80 m amplitude, zero phase) at the lower boundary.

values of refractive index and they tend to avoid regions of lower values. In regions of negative refractive index wave propagation is forbidden; there the solution has evanescent rather than oszillatory behaviour. Even though the WKB approximation does not hold for the planetary waves under consideration, it turns out to be a useful qualitative guide even in this situation (Karoly and Hoskins, 1982). Palmer (1982) shows that for a quantitatively correct expression for the refraction of EP flux trajectories in terms of the refractive index one has to divide the ν_s as defined in equation 3.20 by $(\sin\varphi)^2$ and also use a particular, modified coordinate system. However, the differences arising from these modifications are small for middle and high latitudes and do not affect our qualitative discussion. We therefore stick to the refractive index as defined in chapter 3 and the physical (φ, z)–coordinate system.

A strong westerly jet with strong meridional curvature turns out to be an important feature of the basic state wind field (Matsuno, 1970; Simmons, 1974; Karoly and Hoskins, 1982; Lin, 1982). Such a jet-like feature yields a ridge-like structure in the refractive index, mainly through the meridional curvature of the wind field. This ridge acts as an upward wave guide for the waves propagating from below, which otherwise would be refracted towards the equator. A strong westerly jet, therefore, can lead to increased wave amplitude in the higher stratosphere. In this sense the effect of strong curvature in the basic state wind field can override the effect of large wind speeds (Lin, 1982).

In fact, in our present case the westerly jet does produce a ridge in refractive index in higher latitudes (see figure 4.3). The maximum values of this ridge are between 25 and 35 for all months. However, in the early months (April and May) the ridge does not reach down all the way to the forcing level (200 mb). In addition, in early months the local low altitude minimum is positioned in rather high latitudes ($\varphi \simeq -56°$ in April). In later months, this minimum shifts towards lower latitudes ($\varphi \simeq -38°$ in September) and the ridge "gains contact" with the forcing level. The exact location of the minimum may be essential, since low values of refractive index inhibit wave propagation. According to Lin (1982) the local minimum bifurcates the wave into an equatorward branch and a poleward branch, of which only the poleward branch can contribute to a substantial wave amplitude in the higher stratosphere. Another presumably important feature in refractive index is the poleward gradient of refractive index, which is established through the configuration of the midlatitude minimum and the higher latitude ridge. Again,

this gradient is considerably stronger in low altitudes in later months.

Noting that the latitudinal maximum of the forcing lies around $\varphi \simeq -60°$ (see figure 3.2), it appears plausible that the response of the wave is particularly sensitive to the low altitude refractive index in the neighbourhood of this latitude. Therefore, we plot the refractive index at 100 mb for latitudes between $-80°$ and $-40°$ in figure 4.12. In fact, there is a qualitative similarity of this plot and the seasonal cycle of the wave in the higher stratosphere (figure 4.5, lower two panels). In addition there is a correlation between months with strong amplitude and months with strong poleward gradient in refractive index around $-50°$ latitude. Therefore we suggest that the *essential features in the (low level) refractive index field for wave propagation* can be summarized as follows:

> In order to get strong amplitude in the higher stratosphere, the wind field in the lower stratosphere has to be such that it results in a ridge in refractive index. Since this ridge acts as a wave guide, it should "connect" the low altitude forcing level with the higher stratosphere. Strong poleward gradient in refractive index in mid-latitudes enhances the strength of the wave guide, while a local minimum in refractive index may inhibit upward wave propagation through its specific location. The ridge works particularly efficiently if it coincides in latitude with the latitude of maximum forcing.

Another feature of importance is presumably the midlatitude minimum (with negative values) in refractive index around the 1 mb level in September and October. As suggested by Matsuno (1970) this minimum acts as a barrier for wave propagation and thus creates a *cavity like structure*, which might lead to resonance. It gives a plausible "explanation" for why the maximum in wave amplitude shifts downward in these months, and why the amplitudes are relatively strong. Both the downward shift and the relative strength is in good agreement with the observations.

With these "rules" the seasonal cycle of the model wave can be interpreted in an internally consistent way. In particular, the missing of the observed amplitude maximum in early winter is plausible.

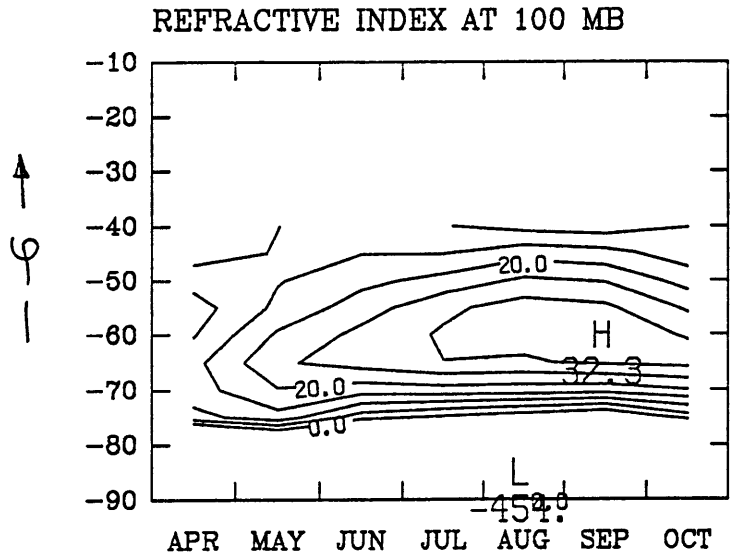

Figure 4.12: Seasonal cycle of the refractive index at 100 mb for latitudes between $-80°$ and $-40°$. Contour interval: 5. Only non-negative contours are drawn.

4.3.2 Wave structure in the meridional plane

There is a striking similarity in the structure (in particular the meridional structure) of the wave amplitude and the basic state wind in the middle and upper stratosphere for later months (July through October). It seems as if the *shape* of basic state wind field determines to a great deal the *shape* of the wave amplitude. This statement is supported by the fact that it holds for the run with constant forcing (figure 4.9). The differences in forcing show up only in the lower stratosphere, while in the upper stratosphere the shape of the amplitude for both realistic and constant forcing is similar and resembles that of the basic state wind.

This *mimicing behaviour* was clearly pointed out by Simmons (1974) in an analytical study of the linearized quasigeostrophic potential vorticity equation. He shows that on a beta plane for a separable basic state wind of the form $\bar{u}(y,z) = Y(y)Z(z)$ there is an approximate separable solution ψ', which adopts the meridional profile $Y(y)$ of the basic state: $\psi'(y,z) \simeq Y(y)\hat{Z}(z)$. This solution is characterized by an approximate cancellation of meridional curvature terms like $\bar{u}\psi'_{yy}$ and $\bar{u}_{yy}\psi'$ in the vorticity equation. The

approximation requires curvature terms in $\bar{Q}_y$ to dominate the beta term. He shows that his results apply also to polar cap geometry.

In fact, in later months our basic state wind fields have curvatures in the jet region strong enough (see figure 4.2) that the curvature terms dominate the beta term $2\Omega\cos\varphi/a$ $(= \cos\varphi \times 0.23 \times 10^{-10}\mathrm{m}^{-1}\mathrm{sec}^{-1})$ in the expression for $\partial\bar{Q}/\partial(a\varphi)$ (equation 3.6). We also checked the terms that are the spherical analogues to $\bar{u}\psi'_{yy}$ and $\bar{u}_{yy}\psi'$ in our equation, and we found "cancellation" of the order 60% ...90% for later months in the area of the westerly polar night jet. In summary, Simmons analysis is approximately verified in our model and can, therefore, be considered as an explanation of the mimicing behaviour between wave amplitude and basic state wind in regions of strong basic state flow curvature.

4.3.3 Comparison with the Charney-Drazin model

In the introduction we mentioned that Charney and Drazin's simple model suggests a qualitative answer for the observed seasonal cycle with the local wave minimum in midwinter. Accounting only for vertical wave propagation and assuming a constant basic state veolcity $\bar{u}$, their model allows stationary wave propagation only for values of $\bar{u}$ satisfying $0 \leq \bar{u} \leq \bar{u}_{\mathrm{crit}}$ with some $\bar{u}_{\mathrm{crit}}$ (Charney-Drazin criterion). In that case the amplitude grows like $\propto \exp[z/(2H)]$ with height. Otherwise the wave cannot propagate vertically and the solution is evanescent in character. As mentioned in the introduction, A. Plumb (1989a) uses this idea in a simple nonlinear model and shows that one can interpret the minimum in amplitude in midwinter as due to the westerlies becoming too strong.

However, allowing for spherical geometry, flow curvature, and meridional wave propagation requires a few important *modifications* of the Charney-Drazin model leading to effects which are not even qualitatively accounted for by the latter:

1. There is an overall tendency for waves to be refracted towards the equator, which makes the wave grow in altitude less than in the Charney-Drazin model.

2. Strong westerly jets can function as wave guides and focus wave activity

into the higher stratosphere. This means that the effect of strong basic state wind curvature may override the effect of a large absolute wind values.

3. In regions of strong basic state wind curvature (polar night jet) the wave tends to mimic the basic state wind in its structure.

These features were clearly pointed out earlier in the literature (e.g. Karoly and Hoskins, 1982; Lin, 1982). Items 2 and 3 stand in some sense against the simple reasoning à la Charney and Drazin: Strong westerly jet structures can give an enhanced rather than a reduced wave response. In other words, in the present model weak westerly winds (as in April and May) do not necessarily mean strong wave amplitude in the higher stratosphere.

Therefore, it seems somewhat fortuitous that the Charney-Drazin criterion is able to "explain" the observed seasonal cycle. As for the wave propagation, the present model certainly captures some essential features qualitatively correctly, which are not accounted for by the former. Unfortunately, even though the present model appears internally consistent, it disagrees with the observations in the seasonal cycle. The reason therefore is as yet unclear.

Chapter 5

Model sensitivity

The results presented in the previous chapter stem from our model as described in chapter 3. We will refer to these results as the "standard case" or " standard run". Even though the model appears to be internally consistent, it has not yet become clear, how significant the results are. For it is conceivable that the model response is highly sensitive to one or several model parameters or model assumptions. Such a hypothetical high sensitivity would greatly reduce the significance of the results, since some of the model assumptions are rather simplifying, and there is some uncertainty about the input data.

Therefore we investigate the model's sensitivity in this chapter. First we consider more technical details like our treatment of the boundary conditions, sponge layers, critical lines and static stability parameter. In the following three sections we will vary physically more relevant quantities like forcing, damping, and the basic state wind field, and we will study the modified model response. It will be shown that the model sensitivity is generally speaking quite low and that the the results reported in chapter 4 remain valid qualitatively. At the same time we will relate the results for the modified fields to the correspondingly modified diagnostic quantities, which allows us to test the validity of our interpretation from section 4.3.

5.1 Sponge layers, critical levels and static stability

First we double and halve the damping contribution α_2, which acts as sponge underneath the upper boundary of the domain. The resulting wave amplitudes are so similar to the standard run that they are not worth being reproduced here. Quantitatively the difference between the $1/2 \times \alpha_2$ and the $2 \times \alpha_2$ case is at most 6 %.

Similarly, dropping the equatorward sponge α_3 entirely leads to negligible changes in wave amplitude. Quantitatively the $\alpha_3 = 0$ case and the standard case differ at most by 5 %. This at first somewhat surprising result appears plausible if one notices that close to the equator there is a critical line and small basic state velocities for all months under consideration, which leads to enhanced damping. The effect is apparently so strong that is makes the sponge α_3 essentially superfluous.

For a similar reason it comes without surprise that the following change in damping has very little influence. To enhance the damping in the neighbourhood of critical lines, a velocity dependent fourth part α_4 is added to the damping coefficient:

$$\alpha_4 = \begin{cases} \frac{5 \text{ m/s} - |\bar{u}|}{5 \text{ m/s}} \text{ day}^{-1} & \text{for } \bar{u} \leq 5 \text{ m/s} \\ 0 & \text{else} \end{cases} \tag{5.1}$$

The response is again virtually unchanged (maximum change less than 2 %).

In another run the basic state wind field is changed such that critical lines are avoided alltogether. Values of $\bar{u}$ less than + 5 m/sec are substituted by + 5 m/sec, and values of $\bar{u}$ in the range 5 m/sec $\leq \bar{u} \leq$ 10 m/sec are modified such as to guarantee a smooth transition. Again, there is no qualitative change. Quantitatively the response is of the order of 5 % stronger for the midwinter months, 7 % stronger in April, and 15 % stronger in October. This slight increase in wave amplitude can be interpreted in terms of the refractive index. The modification increases the curvature of the basic state wind field in the sense that the midlatitude minimum in refractive index gets more pronounced. This effect blocks wave activity away from the equator and enhances the efficiency of the higher latitude wave guide by increasing the local poleward gradient in refractive index, resulting in a somewhat stronger response

in the higher stratosphere. The effect applies especially for October, since in this month the critical line extends far into the interior of the domain.

In order to get a better feeling for the validity of the sponge layer approach, a Neuman boundary condition is implemented at the upper boundary and the sponge α_2 is dropped. At the same time more realistic basic state winds above 1 mb are used (derived from Marks, 1989). The resulting wave amplitude below 1 mb is again practically undistinguishable from the one obtained with Dirichlet zero boundary condition using the sponge layer (maximum change about 3 %).

So far we paid little attention to the basic state static stability N^2, which is given in terms of the observed temperature field by equation 3.12. The reason therefore is, because the model is very insensitive to the precise structure of $N^2(\varphi, z)$, a result already pointed out by Schoeberl and Geller (1977). Using a constant $N^2 = 4 \times 10^{-4}$ sec^{-2} instead of $N^2(\varphi, z)$ as calculated from the observed temperature field results in a very similar wave response (maximum deviation from the standard case is about 6 %). Similarly the response is virtually unaffected (maximum change about 3 %), if one uses a $N^2(z)$ which depends only on altitude (as maybe most adequate for quasi-geostrophic theory), being defined as the latitudinal average of $N^2(\varphi, z)$ over the latitudes in our domain.

In summary, the model can be regarded as insensitive to those rather technical issues as how precisely we handle boundary conditions, critical levels[1] and the basic state static stability. Therefore we are confident that within the framework of the model assumptions our numerical implementation gives a faithful representation of the model.

5.2 Sensitivity with respect to forcing

Forcing was investigated to some degree in section 4.2, where we showed that its impact is weak in the sense that both the meridional structure and the seasonal cycle of the response is mostly determined by the basic state wind. Later in chapter 4 (section 4.3.1) we found through refractive index analysis

[1] Insensitivity to critical layer treatment has only been shown for entirely absorbing critical layers, an assumption which we make in the present model.

that the wave in the higher stratosphere depends mostly on forcing in mid- and higher latitudes. Both statements are reexamined and qualitatively verified in this section by modifying the forcing at the lower boundary.

First we specify the "realistic" wave amplitude and phase at 200 mb from Randel's data, but only in the latitude rage $-75° \leq \varphi \leq -45°$, and zero amplitude for all other latitudes. This particular latitude range is chosen, because inspection of the wave amplitude at 200 mb (figure 3.2) suggests the distinction of a forcing contribution from mid- and high latitudes and a forcing contribution from low latitudes. Both contributions are separated by a pronounced minimum around $-45°$ latitude for all months.

The amplitude fields (figure 5.1), the seasonal cycle (figure 5.2) and the EP flux diagram (not shown) resulting from this run with restricted forcing show a striking similarity with the standard run. This result suggests that in fact low latitude forcing (which has its maximum around $\varphi \simeq -35°$) hardly contributes to the overall response. The behaviour is consistent with our refractive index interpretation: wave activity from lower latitudes is immediately refracted towards the equator, where it gets absorbed in our model. It is also consistent with the notion developed in section 4.3.1 that the wave in the higher stratosphere is particularly sensitive to to the low altitude refractive index in mid- and high latitudes.

For the late months (in particular September and October) the response is slighly *stronger* (order of 10 %), even though the forcing is restricted to a 30° range in latitude (as opposed to the standard case with forcing over the whole range from $-85°$ to $-15°$). This phaenomenon can be understood in terms of destructive interference: As the respective phase plots (not shown) prove, the contribution from mid- and high latitudes on the one hand, and from the low latitudes on the other hand, are not entirely in phase in the higher stratosphere. Thus the two respective wave contributions do not superimpose entirely coherently, which may result in the observed destructive interference.

The shape determining power of the basic state, which was pointed out in section 4.3.2, is demonstrated by another experiment: realistic forcing is spezified in the low latitude range $-40° \leq \varphi \leq -10°$, and zero forcing is specified at all other latitudes. As expected, the overall response (figure 5.3) is very weak (note the different contouring interval), reaching a maximum of 134 m in September. The interesting fact is that the shape of the response

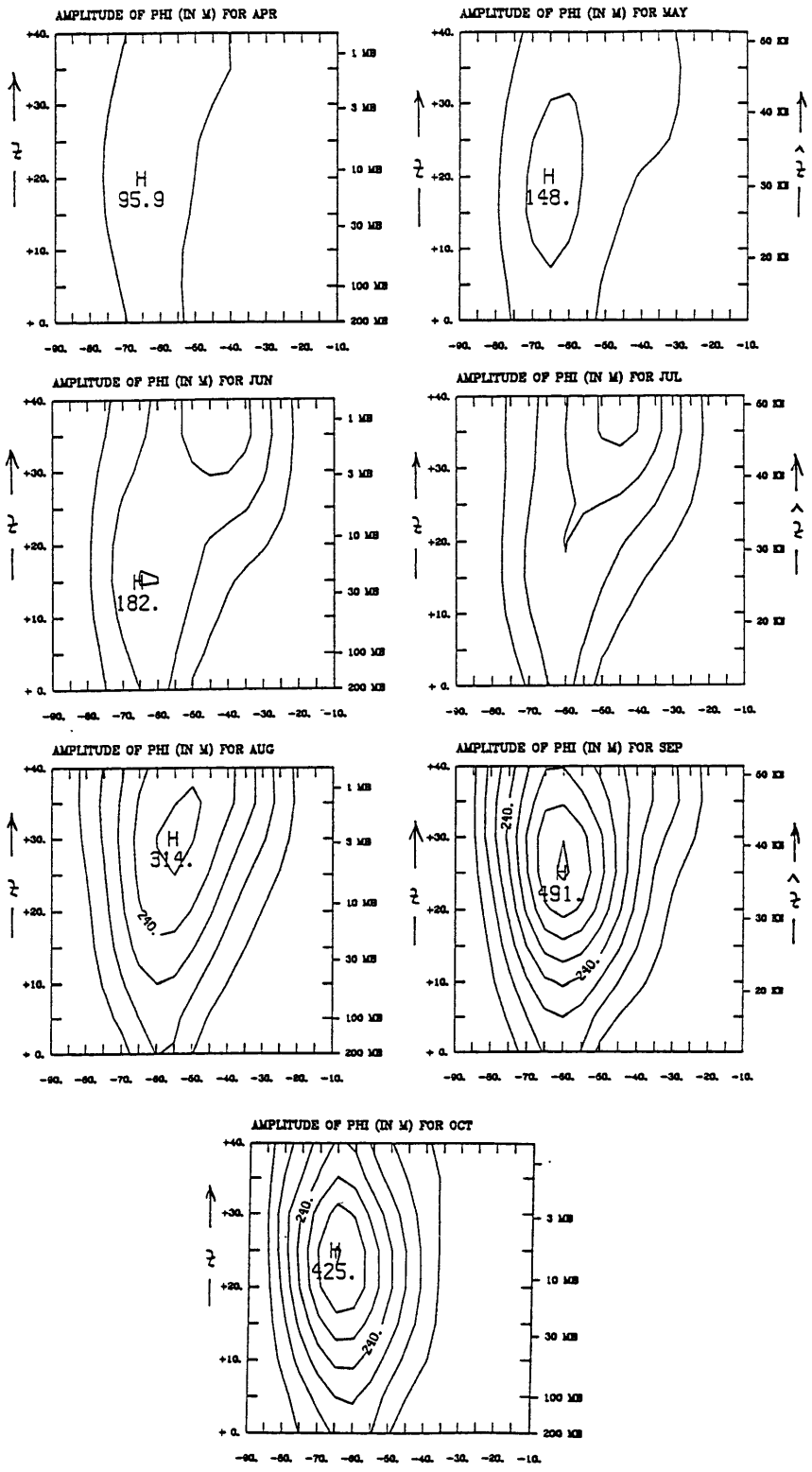

Figure 5.1: Wave amplitude (in geop. m) for forcing only in the latitude range $-75° \leq \varphi \leq -45°$. Contour interval: 60 m. Meridional section. z and $\hat{z}$ in km, latitude in degrees.

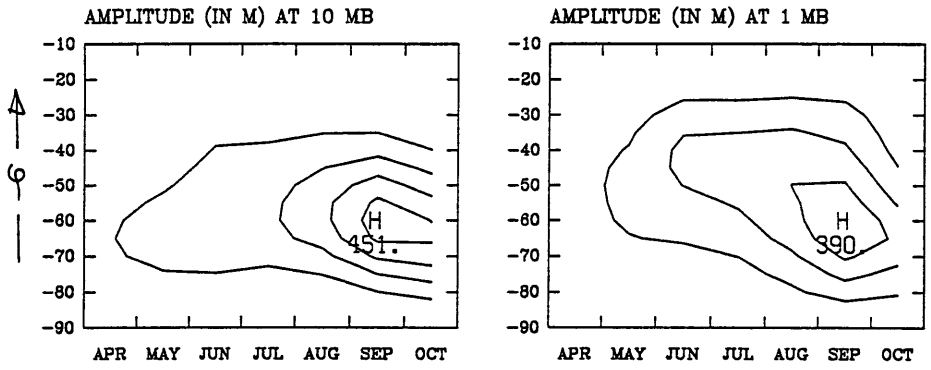

Figure 5.2: Seasonal cycle of wave amplitude (in geop. m) at 10 mb (left panel) and 1 mb (right panel) for forcing only in the latitude range $-75° \leq \varphi \leq -45°$. Contour interval: 100 m.

in the higher stratosphere again "tries" to mimic basic state wind field. The EP flux direction for the low latitude forcing case (figure 5.4) shows again the overall tendency towards the equator, as expected from sphericity and the gross structure of the refractive index.

5.3 Sensitivity with respect to dissipation

The amount of dissipation obviously influences the wave amplitude. In order to get a feeling for how strong the influence is, we halve and double the part α_1 of the damping coefficient, which represents dissipation (Newtonian cooling and Rayleigh friction) in our model. The effect is mainly felt in the higher stratosphere (figure 5.5). Still, the overall meridional (in particular latitudinal) structure is similar to the standard run, and still the response mimics the basic state velocity $\bar{u}$ to some degree.

The seasonal cycle (figure 5.6) is qualitatively unaffected by the variation in dissipation. In order to get a better feeling for the quantitative changes, we plot in figure 5.7 the seasonal cycle of the latitudinal maximum at the 10 mb and the 1 mb level for the different cases. The case with twice (half) the original dissipation is symbolically denoted by $2 \times \alpha_1$ ($1/2 \times \alpha_1$). The solid line refers to the standard case (α_1 unchanged). The variation in dissipation shows up mainly at the 1 mb level. At the 10 mb level only the latest months

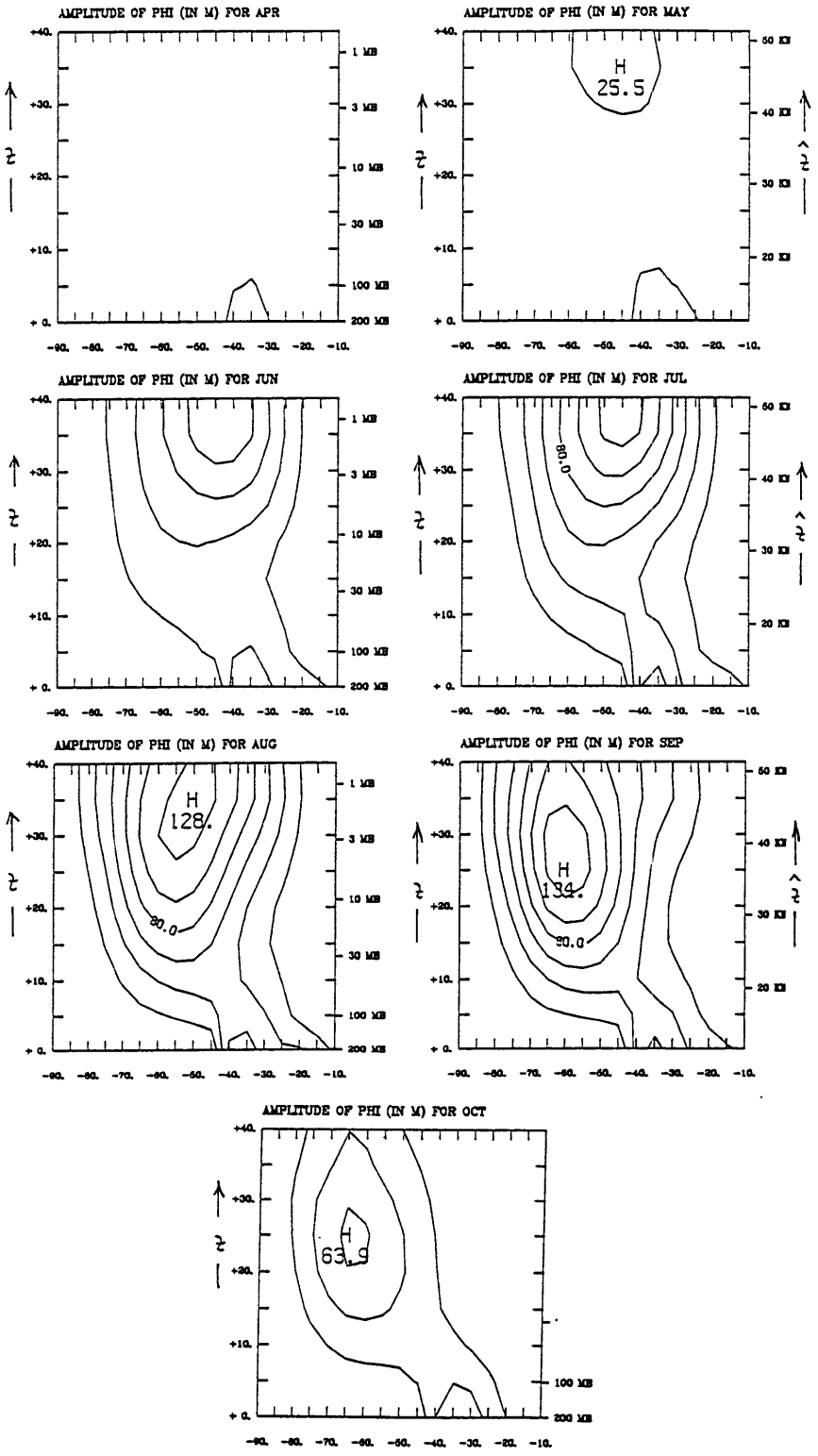

Figure 5.3: Wave amplitude (in geop. m) for forcing only in the latitude range $-40° \leq \varphi \leq -10°$. Contour interval: 20 m. Meridional section. z and $\hat{z}$ in km, latitude in degrees.

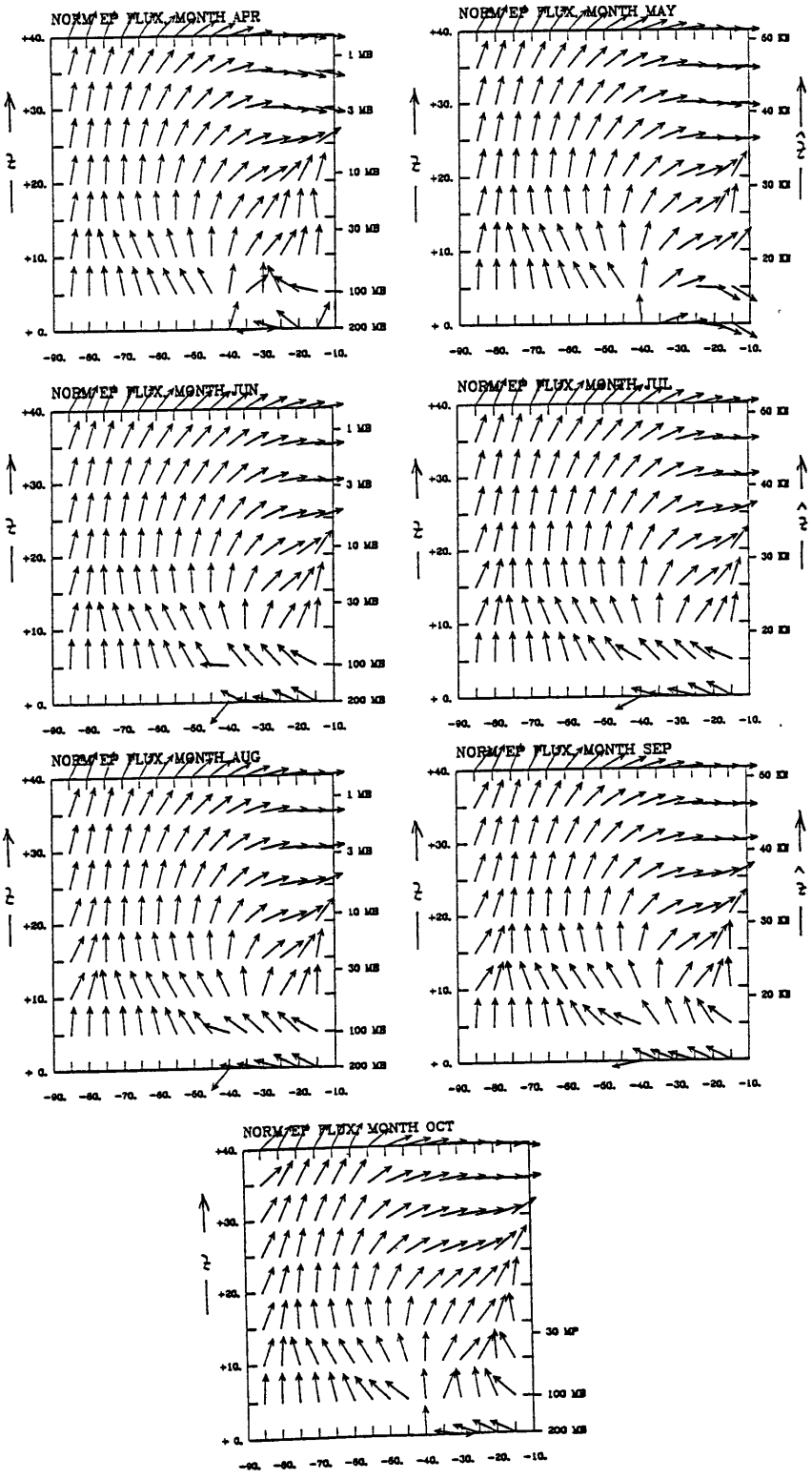

Figure 5.4: Normalized EP flux for forcing only in the latitude range $-40° \leq \varphi \leq -10°$. Meridional section. z and $\hat{z}$ in km, latitude in degrees.

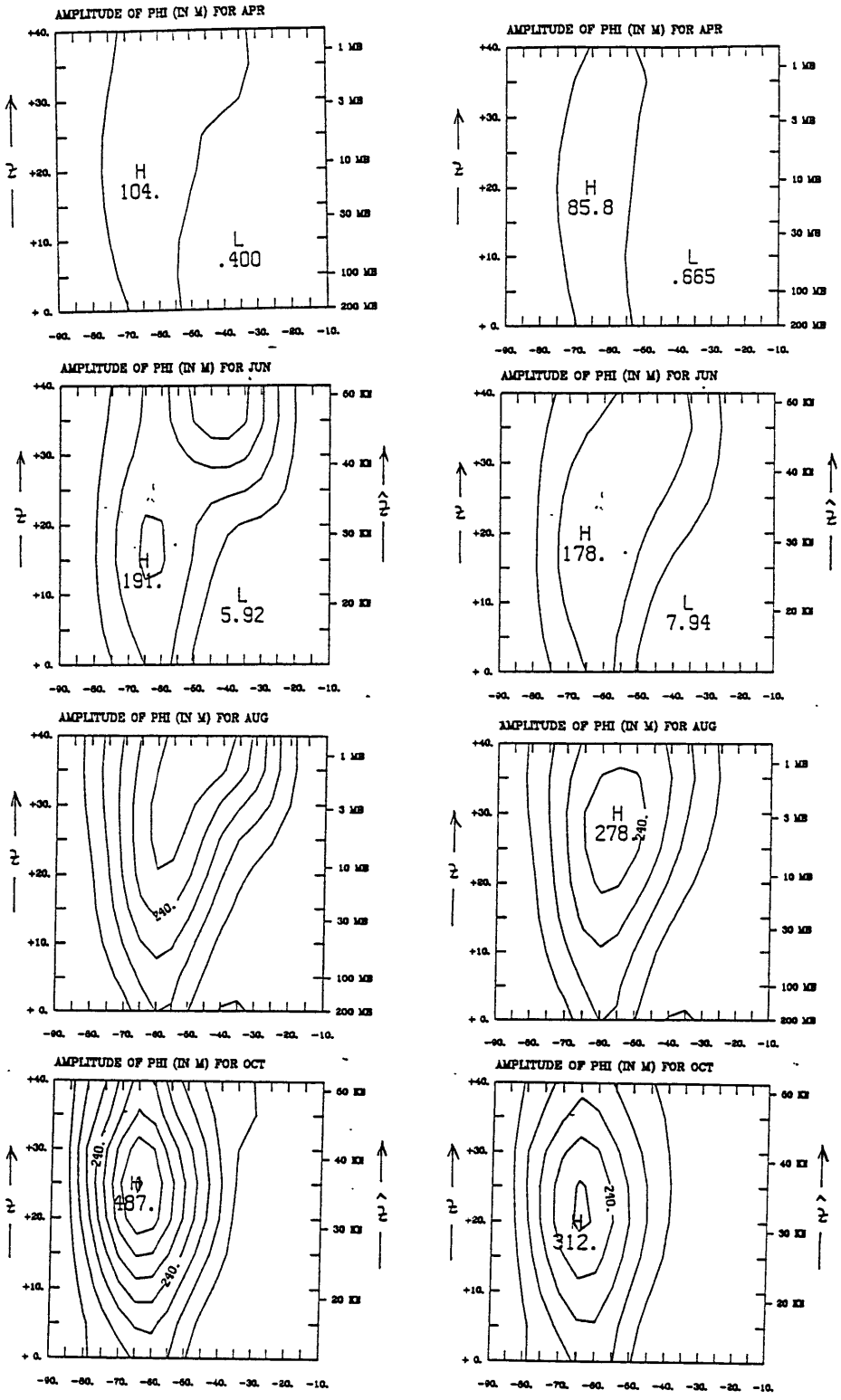

Figure 5.5: Wave amplitude (in geop. m) for half dissipation (left column) and double dissipation (right column). Contour interval: 60 m. Meridional section. z and $\hat{z}$ in km, latitude in degrees.

(September and October) are substantially affected. Quantitatively the difference between the $1/2 \times \alpha_1$ and the $2 \times \alpha_1$ case at 1 mb is within $\pm$ 30 % of the standard case.

In summary, even though there is some quantitative effect (as expected), the qualitative model results are little affected by sizeable variations in dissipation. In particular our statements about the seasonal cycle are insensitive to the exact amount of dissipation.

5.4 Sensitivity with respect to the basic state wind

In this section we study the sensitivity of the model wave with respect to variations in the basic state wind. We distinguish modifications in low levels (i.e. order of 10 km above the forcing level) from modifications that affect the whole domain.

5.4.1 Low level wind modifications

For the low level wind modifications we consider changes of the following form:

$$\bar{u}_{\mathrm{mod}}(\varphi, z) = \bar{u}(\varphi, z) \pm |\sin 2\varphi| \, f(z) \tag{5.2}$$

with some vertical structure function f(z), which is non-zero only in the lowest few kilometers above the forcing level. The addition has a monopole structure with an extremum at $\varphi = -45°$. The precise shape of f(z) does not matter, since the vertical resolution is only 5 km. We choose f(z) such that f = 10 m/sec at the forcing level (z = 0 km) and f = 5 m/sec at the first level above the forcing level (z = 5 km); at all higher levels f is set to zero. The two cases corresponding to the plus or minus sign, respectively, are referred to as *increased* or *decreased low level winds* and denoted as "$\pm$10". A change of the mean zonal wind of the order of 10 m/sec around the 200 mb level can be considered as sizeable: substantially larger changes should be easily detectable by observations and can therefore be savely excluded from our considerations. The same modification as in equation 5.2 with half the amplitude (i.e. f(z = 0 km) = 5 m/sec and f(z = 5 km) = 2.5 m/sec) is referred to as the cases "$\pm$5".

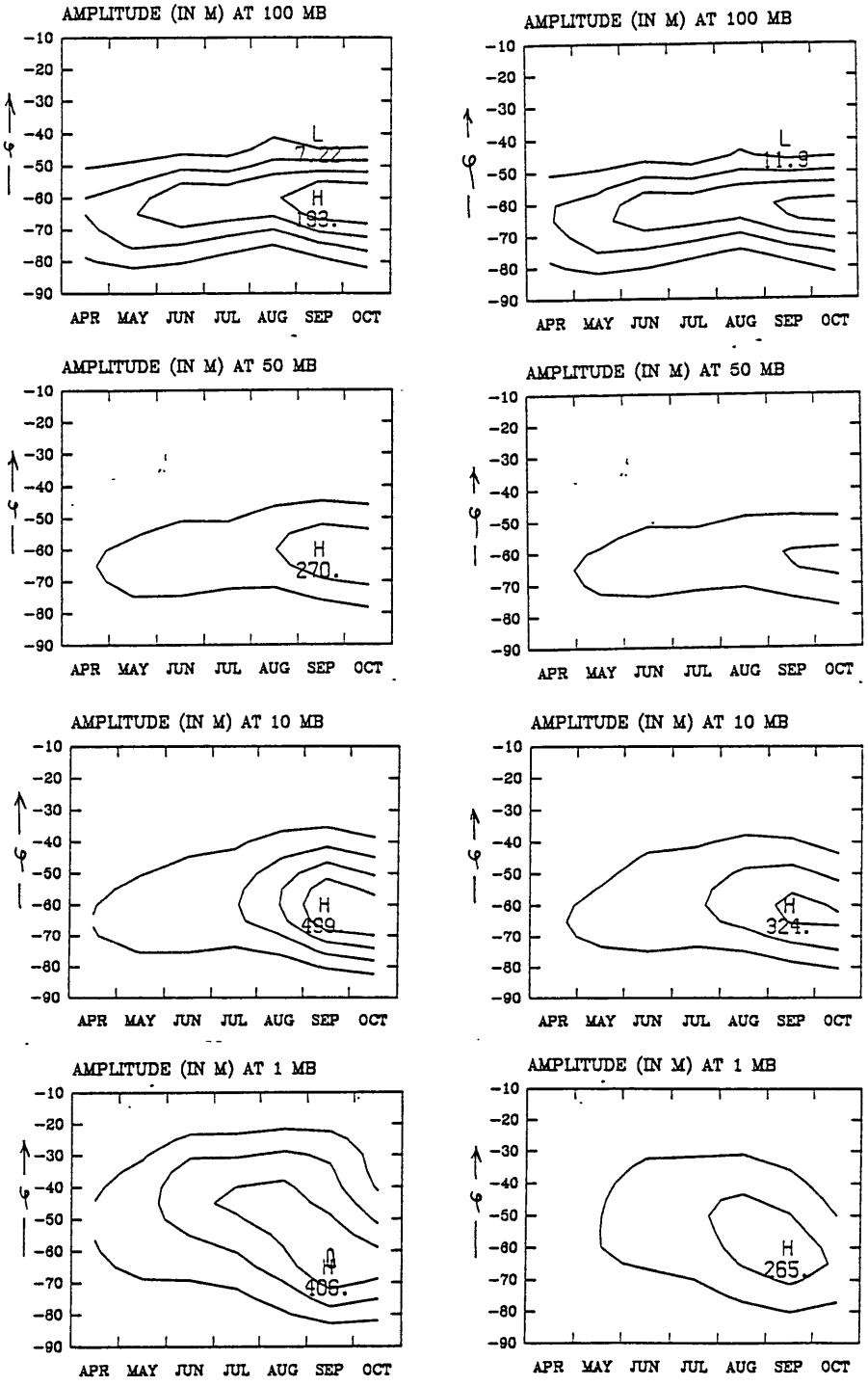

Figure 5.6: Seasonal cycle of wave amplitude (in geop. m) at different pressure levels for half dissipation (left column) and double dissipation (right column). Contour interval: 40 m at 100 mb, otherwise 100 m.

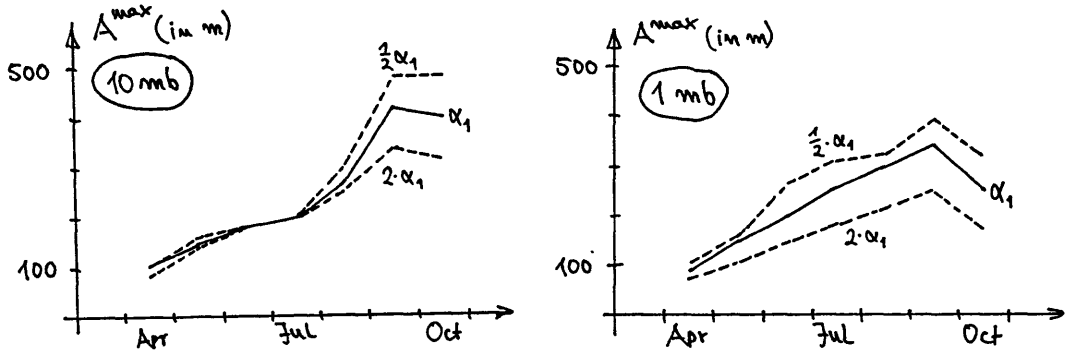

Figure 5.7: Seasonal cycle of the latitudinal maximum of wave amplitude (in geop. m) at 10 mb (left panel) and 1 mb (right panel) for half (upper dashed line), standard (solid line) and double (lower dashed line) dissipation.

At first sight, the modification in the basic state wind field for the "−10" case (figure 5.8) seems not very significant. Obviously the refractive index is a more sensitive quantity, and therefore the change shows up much more clearly in this diagnostic (figure 5.9). The ridge-like wave guide is considerably stronger in low altitudes than in the standard case. This can also be seen in the seasonal cycle of the refractive index at 100 mb as given in figure 5.10, left panel. The qualitative structure has remained similar, but quantitatively the values are larger.

The wave amplitude resulting from the present decrease in low level winds (figure 5.11) is overall stronger in magnitude, but remains unchanged in both its meridional structure and its seasonal cycle. The EP flux direction (not shown) is hardly affected by the modification and therefore proves again to be a fairly insensitive diagnostic. Yet, a closer examination shows that the EP flux vectors are slightly stronger aligned in the vertical direction than in the standard case, which supports the interpretation in terms of the stronger vertical wave guide.

Increasing instead of decreasing the low level winds (+ sign in equation 5.2) leads — mutatis mutandis — to exactly the same results: While the change in the wind field appears modest, there is a considerable change in refractive index, this time being a significant decrease of the higher-latitude ridge (see figure 5.10, right panel). The corresponding wave amplitude is weaker uniformly through all months, while its meridional structure and its seasonal cycle

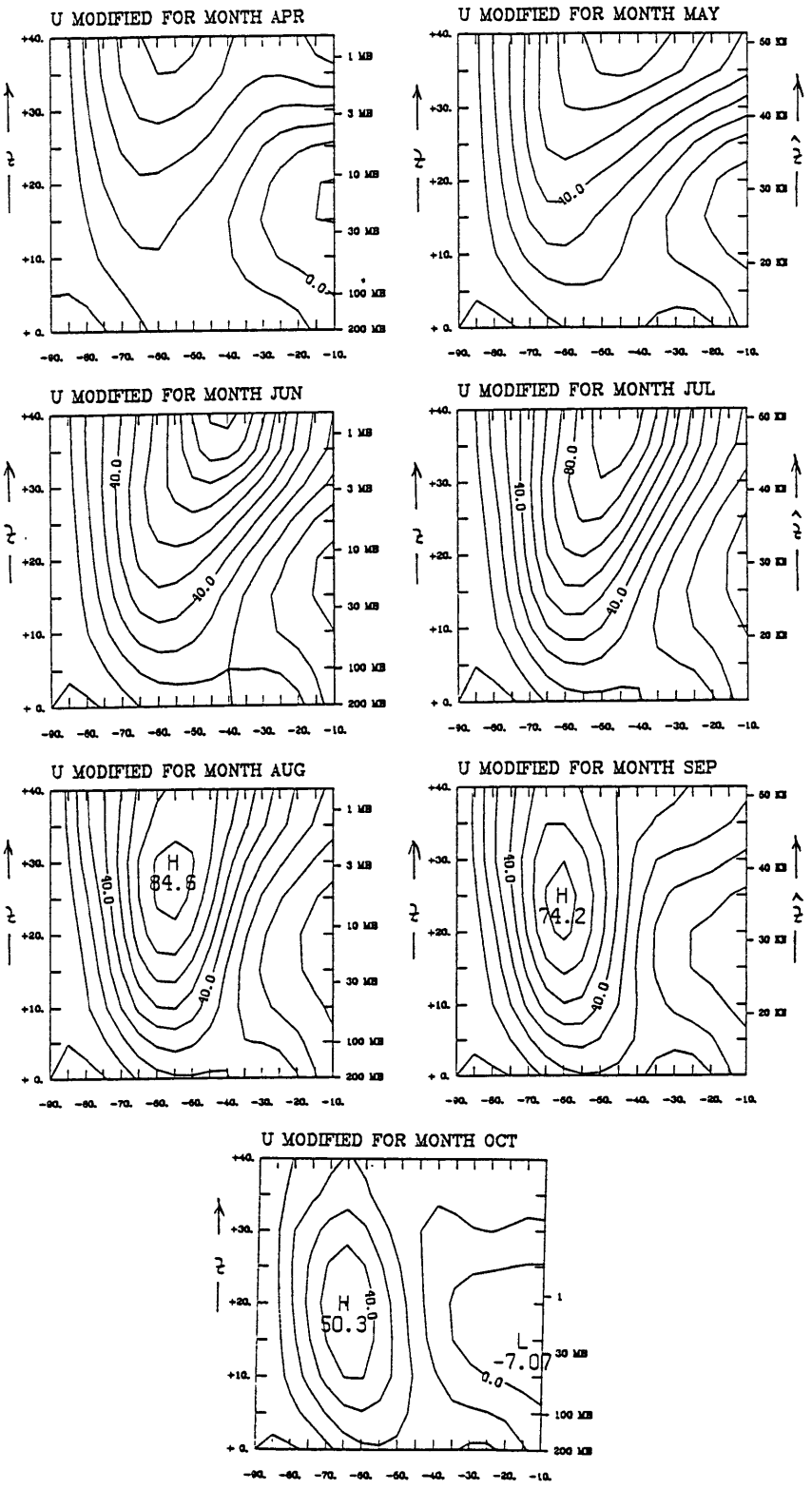

Figure 5.8: Modified basic state zonal wind (in m/sec). Modification: decreased low level winds (case "-10"). Contour interval: 10 m/sec. Meridional section. z and $\hat{z}$ in km, latitude in degrees.

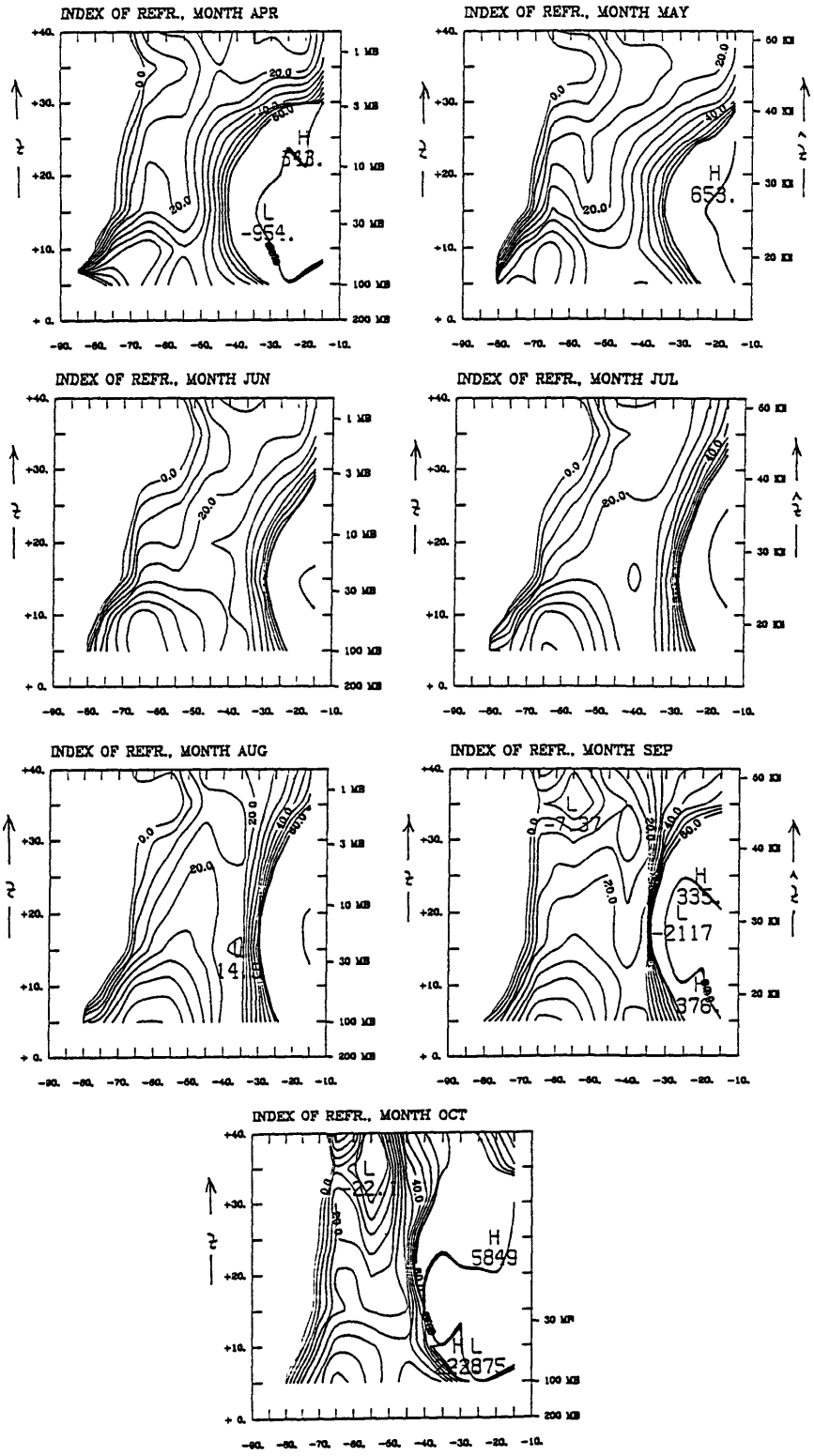

Figure 5.9: Refractive index for modified basic state with decreased low level wind (case "-10"). Only contours between +0 and +60 are drawn. Contour interval: 5. Meridional section. z and $\hat{z}$ in km, latitude in degrees.

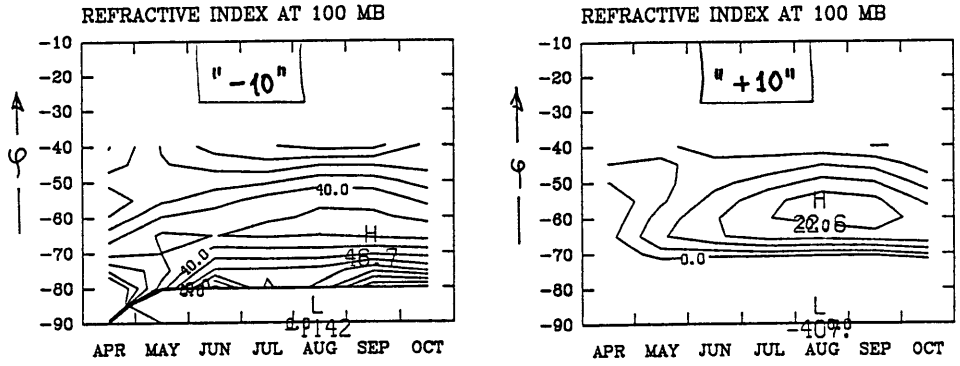

Figure 5.10: Seasonal cycle of refractive index at 100 mb in the latitude range $-80° \leq \varphi \leq -40°$ for decreased ("-10", left panel) and increased ("+10", right panel) low level basic state wind. Contour interval: 5. Only non-negative contours are drawn.

are, again, qualitatively unaffected. Applying the considered modification with half the amplitude (i.e. the "±5" cases) leads to results which lie essentially in between the respective larger modification and the standard case.

To summarize the low level wind modifications, we plot the seasonal cycle of the latitudinal amplitude maximum at 1 mb for the the four cases "±10" and "±5" in figure 5.12. Since neither the meridional structure nor the seasonal cycle changes considerably for these modifications, this plot represents a meaningful quantification of the changes. It shows that the response to changing the low level basic state winds by ±10 m/sec leads to a variation in wave amplitude of the order ± 50 %.

These results can be reduced to our consistent model interpretation from section 4.3 in the following way. Decreased (increased) low level winds lead to increased (decreased) refractive index. Apparently in the expression for the refractive index (equation 3.20) the change of $|\bar{u}|$ in the denominator dominates the change in curvature, which appears in the numerator. This strengthens (weakens) the higher latitude ridge-like wave guide, whence the wave response in the higher stratosphere becomes stronger (weaker). The seasonal cycle in amplitude still reflects reasonably well the low level refractive index around the maximum forcing latitudes ($\varphi \simeq -60°$). The cavity like structure in late months mentioned in section 4.3.1 favours strong amplitudes. This might explain why the amplitude has its maximum in September, while the maximum low level refractive index lies in August (figure 5.12). The

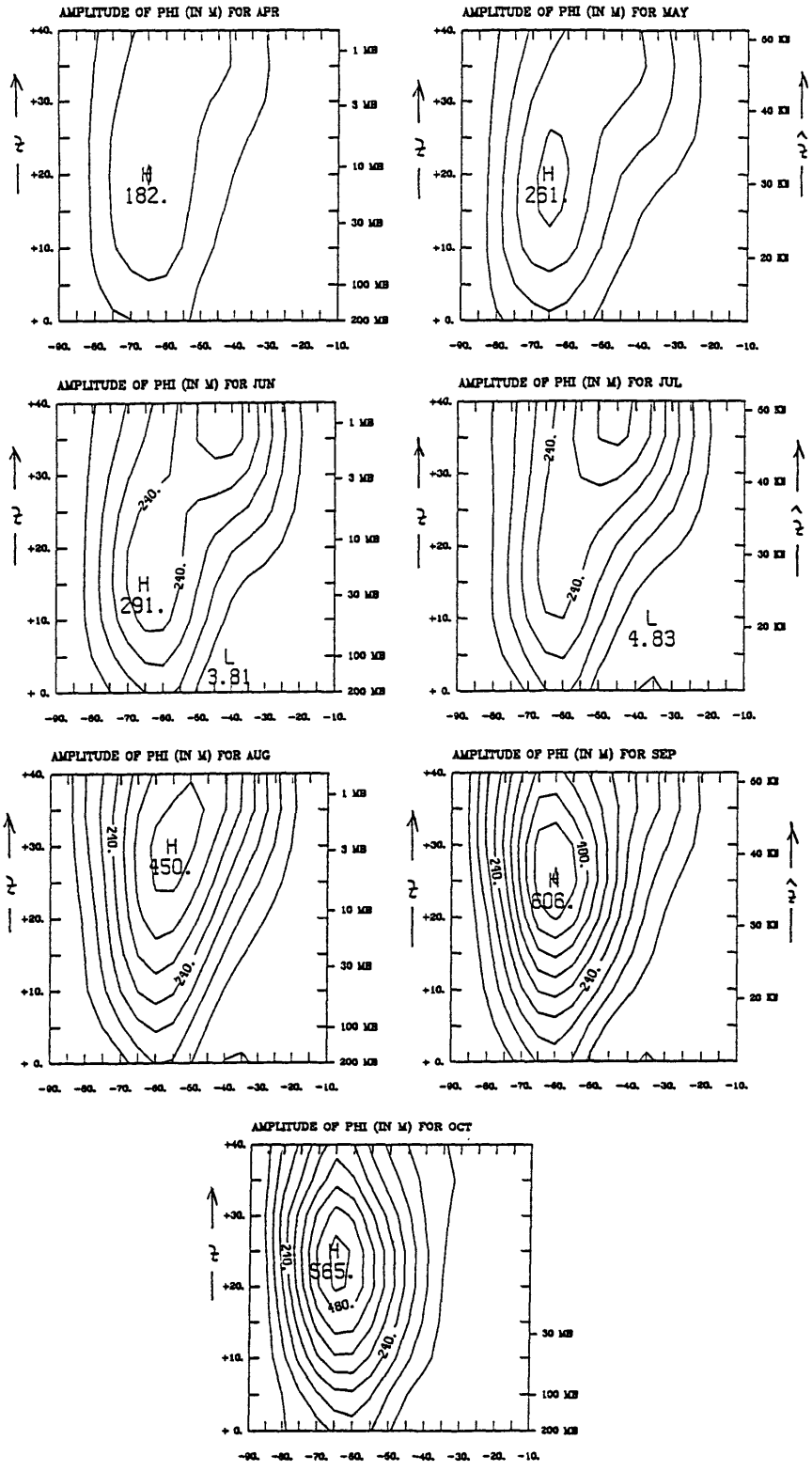

Figure 5.11: Wave amplitude (in geop. m) for for modified basic state with decreased low level wind (case "-10"). Contour interval: 60 m. Meridional section. z and $\hat{z}$ in km, latitude in degrees.

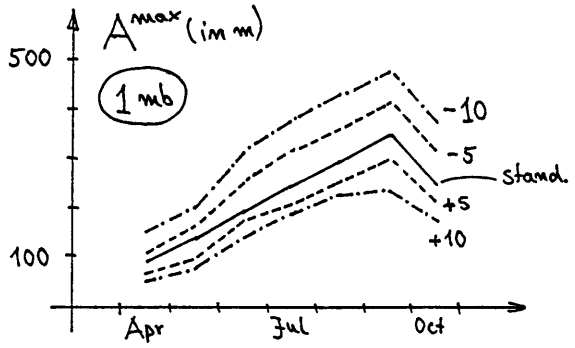

Figure 5.12: Seasonal cycle of the latitudinal maximum of wave amplitude (in geop. m) at 1 mb for the low level basic state modifications (dashed lines) denoted as "±10" and "±5" (see text). Solid line: unmodified standard case.

meridional structure of the wave in the higher stratosphere is not affected by the present modifications, since it is mainly determined through the wind field in this region, which has not been modified.

The sensitivity to low level winds can be used to test the suggested interpretation from section 4.3.1 in yet another way. We modify each month differently according to the following *mixed scheme*: April ("-5"), May ("-10"), June ("-10"), July (unmodified), August ("+10"), September (unmodified) and October (unmodified). This choice is made to produce a double peaked structure in the low level refractive index (figure 5.13): the reduced low level winds in early winter lead to enhanced low level refractive index, while the increased low level winds in August lead to a minimum in low level refractive index in that month. In agreement with the proposed key sensitivity to the low level refractive index, the wave response to these modified wind fields shows indeed a double peaked structure, too (figure 5.14). Thus, again, the model proves to be internally consistent.

It is tempting to interpret this result as follows: Due to the sensitivity of the wave response to variations in the low level wind, the discrepancy between our model wave amplitudes and the observed wave amplitudes can be attributed to uncertainties in the observations. This may be, in fact, partly the case. However, we want to emphasize that the model still reproduces certain qualitative features rather poorly. For instance, the location and relative strength of the two wave maxima at 1 mb in figure 5.14 differ considerably

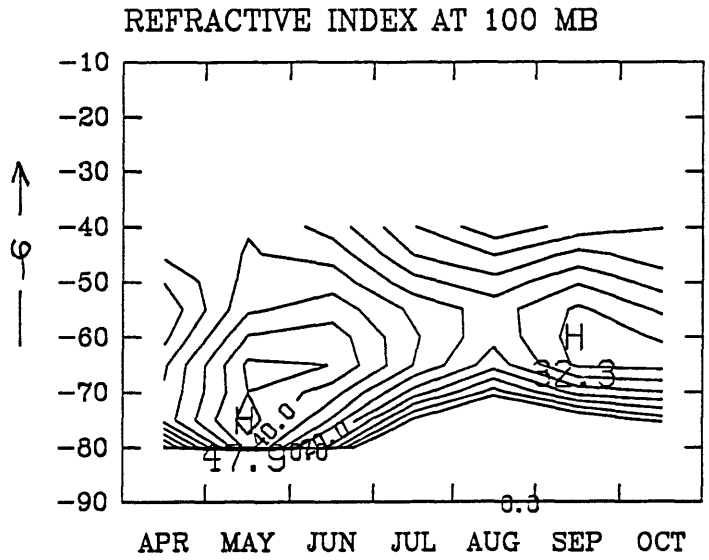

Figure 5.13: Seasonal cycle of refractive index at 100 mb in the latitude range $-80° \leq \varphi \leq -40°$ for low level wind modifications accorcing to the "mixed scheme" (see text). Contour interval: 5. Only non-negative contours are drawn.

from what is being observed (see figure 2.3). Similarly, the wave amplitude in the meridional section for the "mixed scheme" (figure 5.15) shows qualitative discrepancies with the observations (figure 2.4). The observed growth of the amplitude with height in April and May, for instance, is not reproduced by the model.

In summary, the fact that we are able to "generate" in an "engineering approach" (through wind field modifications) a double peaked structure in the wave amplitude at some pressure level in a latitude-time section (as in figure 5.14) at best proves internal consitency of our model and its interpretation. It does not really resolve all discprepancies between our model results and the observations.

5.4.2 More general wind modifications

Finally we study modifications in the basic state wind field that affect more or less the whole stratosphere. There is obviously a lot more potential for different behaviour, but in the most cases we will still be able to interpret

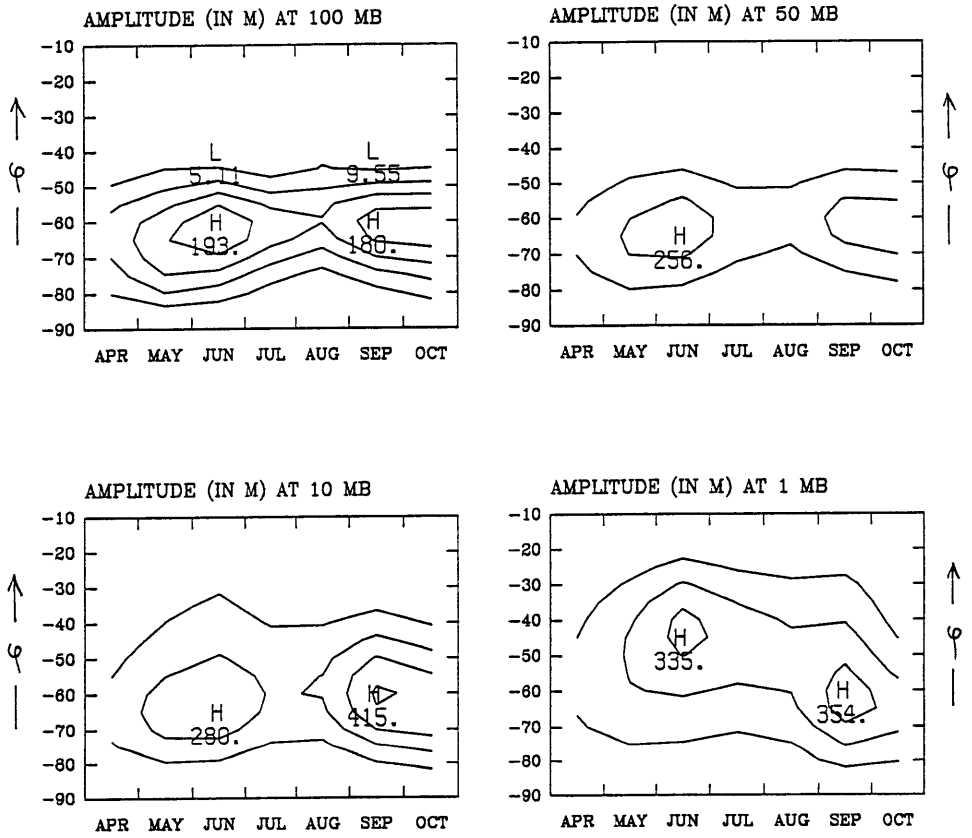

Figure 5.14: Seasonal cycle of wave amplitude (in geop. m) at different pressure levels for low level wind modifications according to the "mixed scheme" (see text). Contour interval: 40 m at 100 mb, 100 m otherwise.

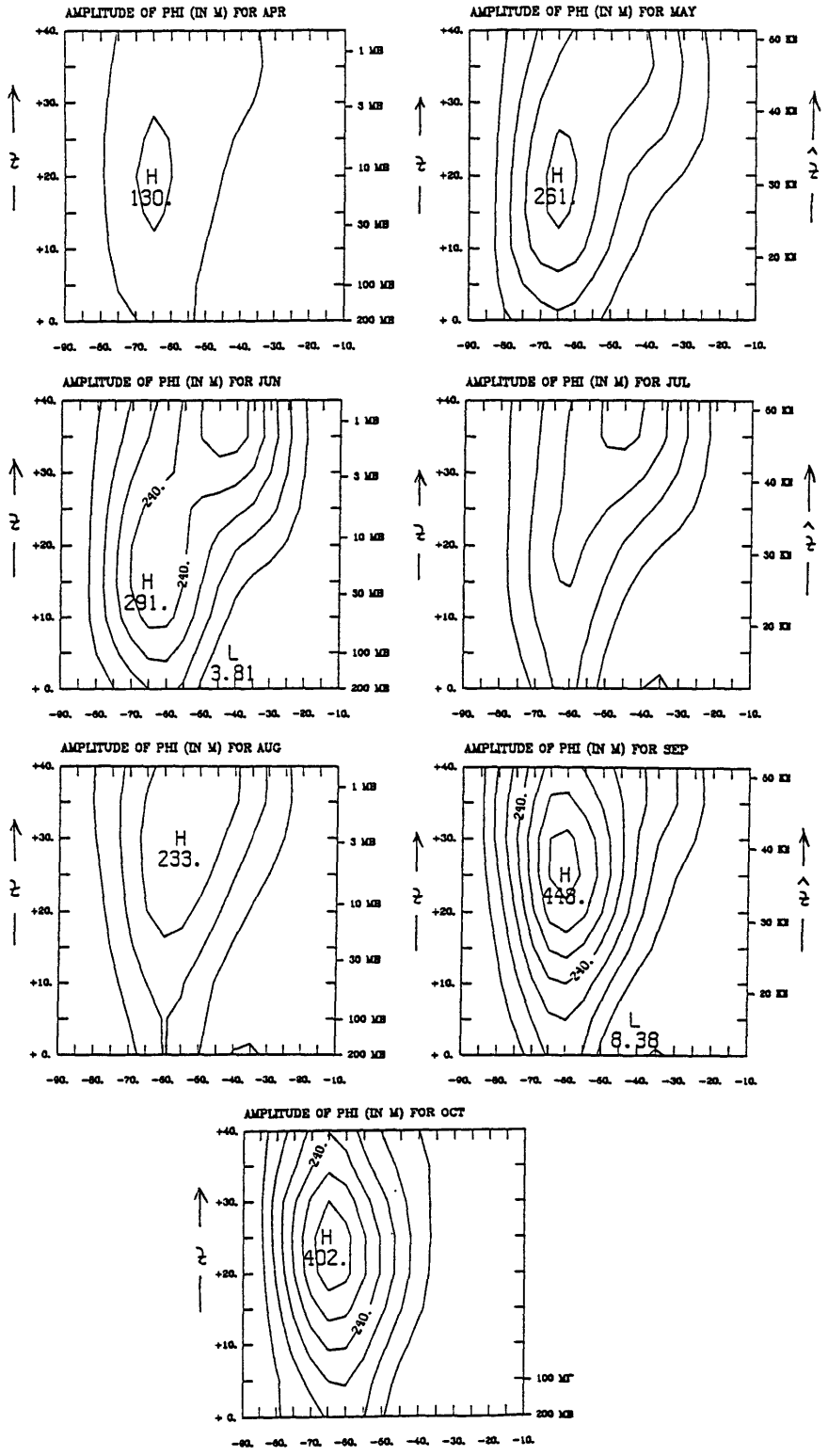

Figure 5.15: Wave amplitude (in geop. m) for low level wind modifications according to the "mixed scheme" (see text). Contour interval: 60 m. Meridional section. z and $\hat{z}$ in km, latitude in degrees.

the results in terms of the refractive index and the mimicing tendency in the higher stratosphere, as described in section 4.3.

First we modify the basic state wind through the whole domain in the sense that the wind field is distorted in the meridional direction according to

$$\bar{u}_{\mathrm{mod}}(\varphi, z) \;=\; \bar{u}(\hat{\varphi}, z) \tag{5.3}$$

with

$$\hat{\varphi} = \varphi - 5^\circ \sin[4.5(\varphi + 10^\circ)] \tag{5.4}$$

The modified wind field (figure 5.16) has a more pronounced jet structure with stronger meridional curvature. We call this modification: *narrower jets.* To some degree this might be a more realistic representation of the zonal wind field at a particular latitude, since zonal averaging should in general lead to broadening of latitudinally narrow features.

The refractive index belonging to this modification (figure 5.17) shows qualitatively the same features as for the unmodified wind. However, both the higher latitude ridge and the midlatitude minimum are considerably more pronounced (mostly in the later months), and the gradient between the local minimum and the ridge is substrantially stronger. This should increase the wave guide property.

In fact, while the meridional structure of the calculated wave (figure 5.18) is qualitatively the same as for the unmodified wind, it has dramatically changed in magnitude in the later months. In particular the amplitude maximum in October has more than doubled, presumably since due to the stronger wave guide into the higher stratosphere the cavity type structure and its concomitant resonant behaviour can work more efficiently. On the other hand, the response in April is almost unchanged. The latter can be rationalized on the basis of the refractive index: the admittedly higher values of refractive index in the midstratospheric ridge still do not reach down to the forcing level, and in particular the gradient between the minimum around -55° and the ridge is very small. Such a structure has to be considered as a weak wave guide, and therefore the waves are refracted right away into the absorbing equatorial region.

In summary we find that "narrower jets" can produce stronger wave guides leading to considerably stronger wave response. The meridional wave structure does not change. Quantitatively the effect is almost negligible in

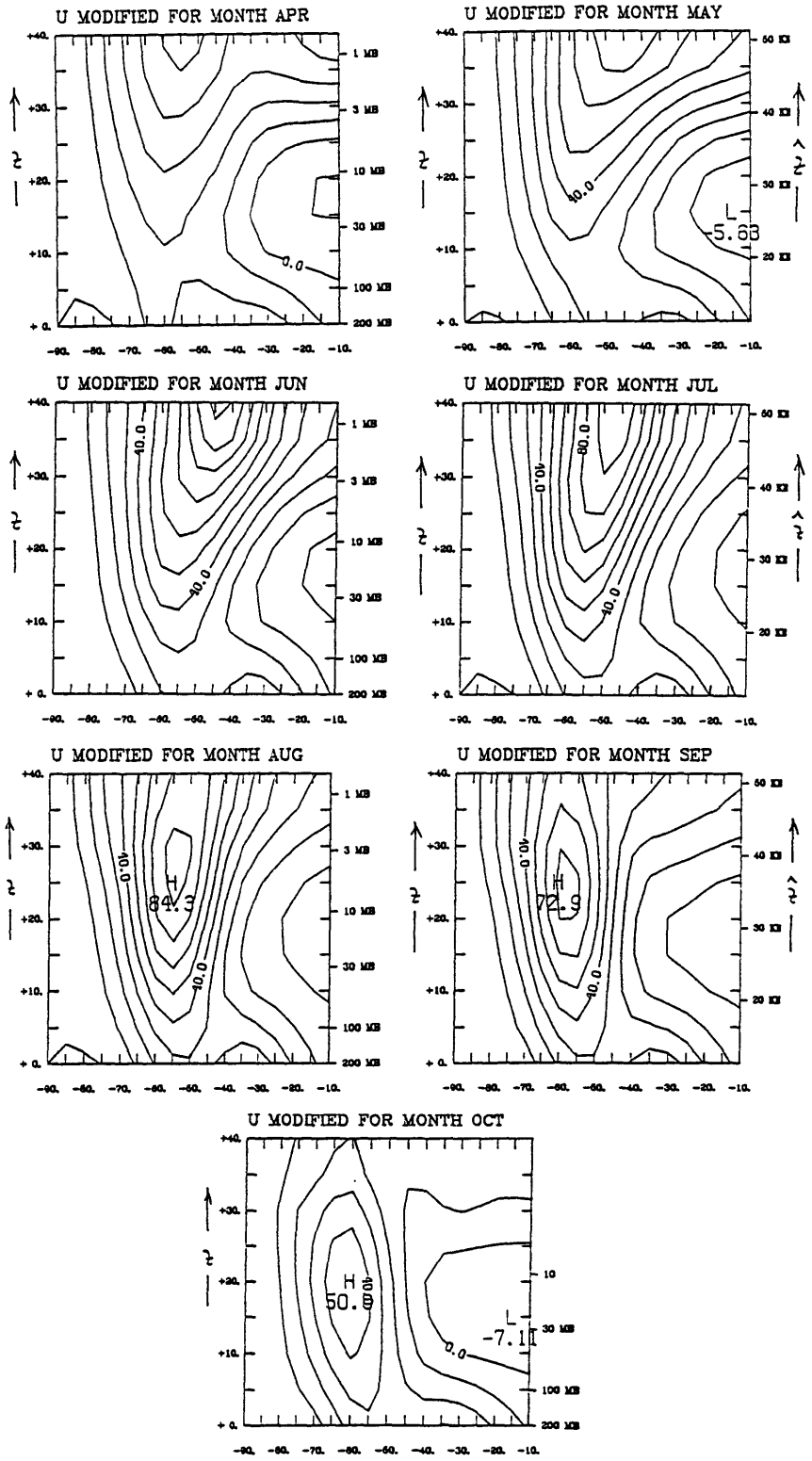

Figure 5.16: Modified basic state zonal wind (in m/sec). Modification: narrower jets (see text for details). Contour interval: 10 m/sec. Meridional section. z and $\hat{z}$ in km, latitude in degrees.

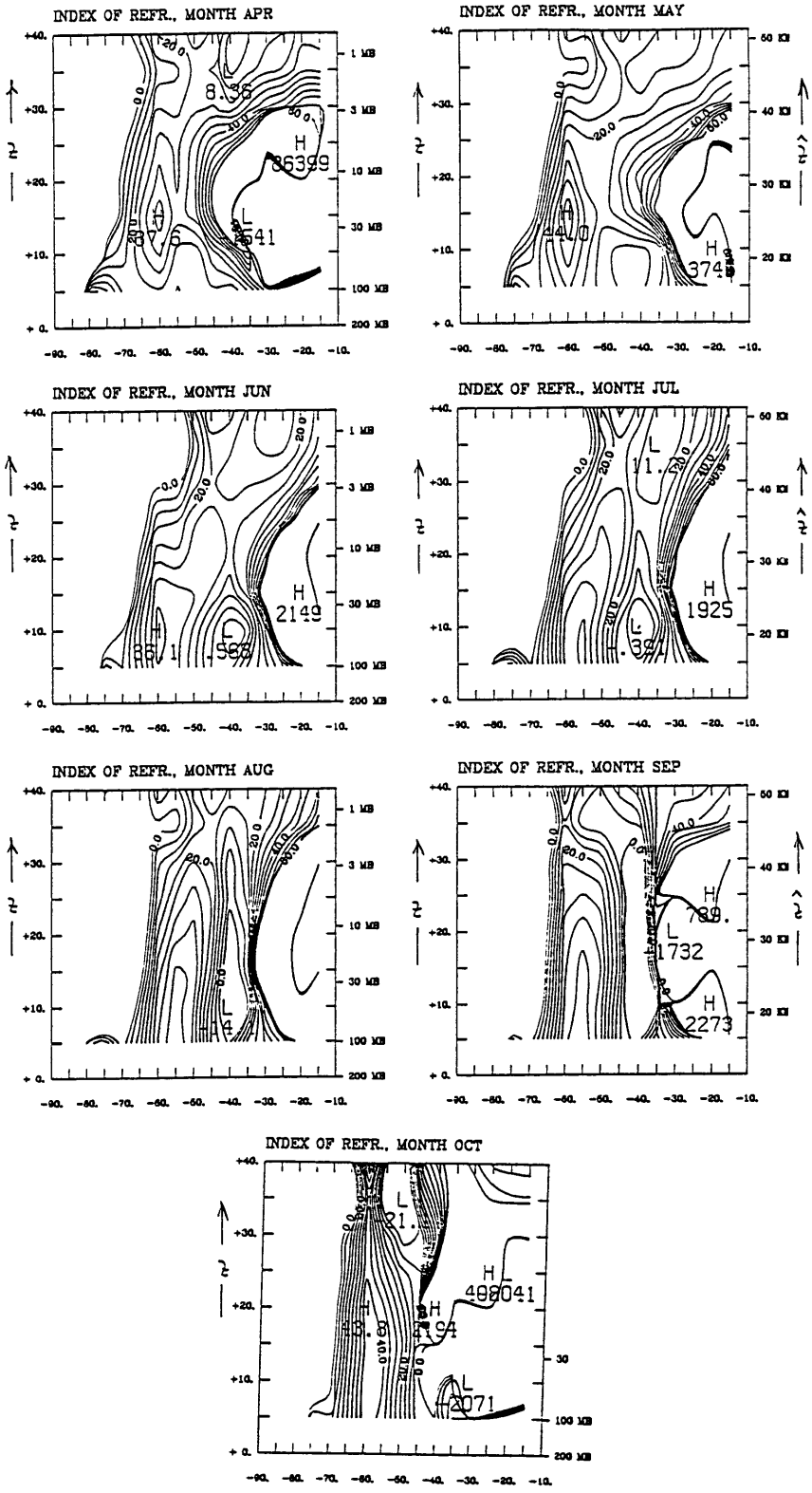

Figure 5.17: Refractive index for modified basic state with narrower jets (see text for details). Only contours between +0 and +60 are drawn. Contour interval: 5. Meridional section. z and $\hat{z}$ in km, latitude in degrees.

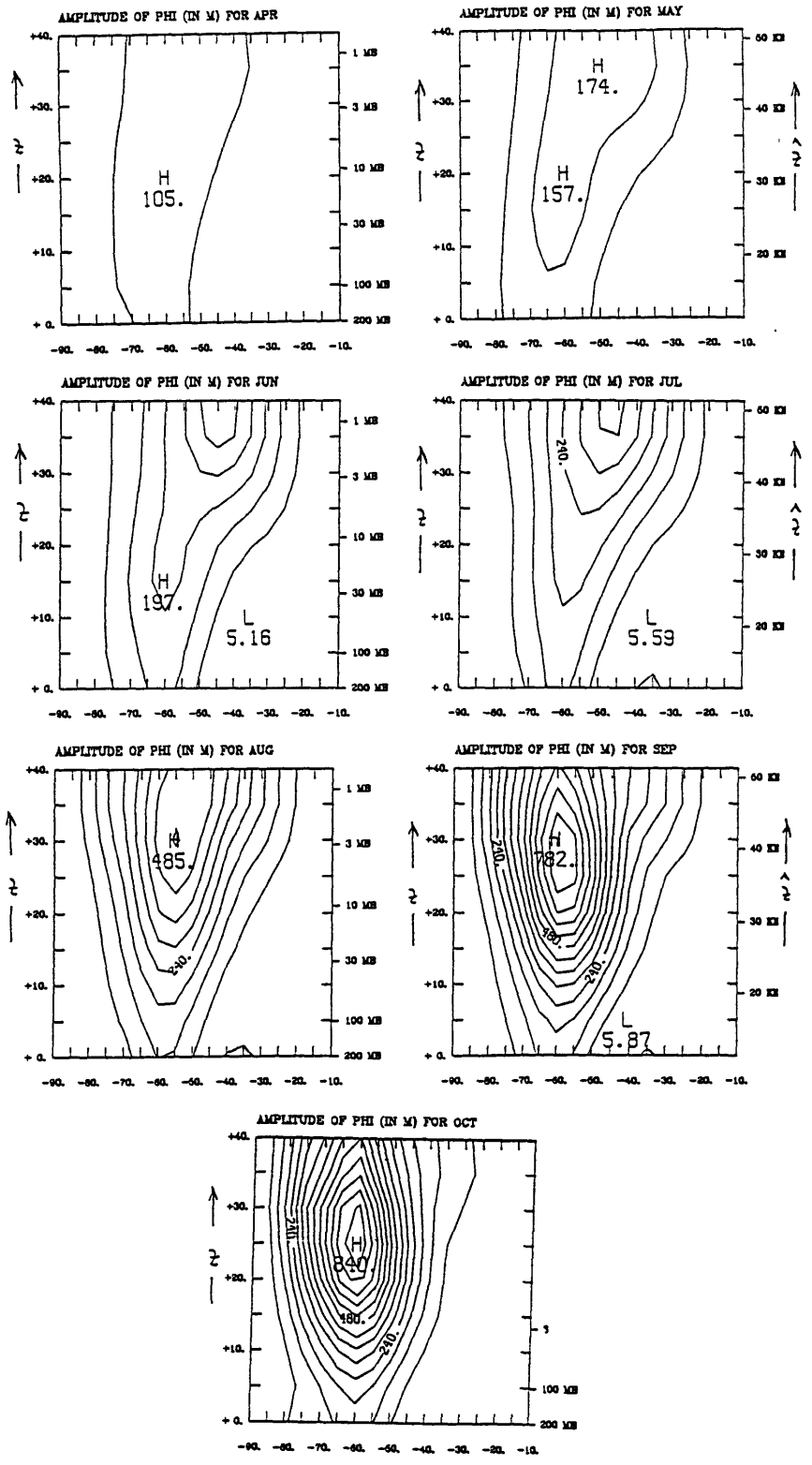

Figure 5.18: Wave amplitude (in geop. m) for for modified basic state with narrower jets (see text for details). Contour interval: 60 m. Meridional section. z and $\hat{z}$ in km, latitude in degrees.

April, but increasingly stronger in later months. Therefore, the seasonal cycle is somewhat distorted in the sense that the late winter maximum gets considerably more pronounced. The stronger wave response due to a narrower jet structure is also in good agreement with earlier studies (e.g. Lin, 1982).

As a second modification we consider a *locally stronger jet*: We add to the original wind profile a "bump" with a maximum strength of 20 m/sec, centered at ($z = 20$ km, $\varphi = -65°$) and with half widths of ($\Delta z = 20$ km, $\Delta\varphi = 25°$). The resulting modified zonal wind, refractive index and wave amplitude are shown in figures 5.19, 5.20 and 5.21, respectively. Compared with the standard case in August the jet maximum increases and descends by about 5 km, while in October the location of the jet maximum does not change (it only increases in magnitude), since in the latter month the bump added coincides with the original jet maximum. Correspondingly the maximum in wave response in August descends by about 5 km with respect to the standard case, while in October its location remains unchanged. This is another example for the tendency of the wave to mimic the basic state wind field.

The most prominent changes in refractive index for the present case of "locally stronger jets" occur in the lower stratosphere. It is again possible (no plots shown) to rationalize the seasonal cycle qualitatively through the refractive index at 100 mb (in connection with the cavity type structure in September and October).

Having studied a large number of further modifications, we often find the following behaviour: as long as the modification directly affects the low level winds or the refractive index in the lower stratosphere, the resulting change in wave response can be qualitatively inferred from the results of section 4.3.1. Changes arising from wind variation in the middle or upper stratosphere are less predictable, but often the wave tries to mimic the wind field. Both effects (low level and higher level modifications) can be "superimposed". For example, strengthening the higher stratospheric jet and decreasing the low level winds at the same time leads to a stronger increase in wave amplitude than each of these modifications individually.

From this point of view the following experiment is interesting. As modified basic state wind we choose half and double the wind from the standard case, i.e. $\bar{u}_{\mathrm{mod}}(\varphi, z) = 0.5\bar{u}(\varphi, z)$ and $\bar{u}_{\mathrm{mod}}(\varphi, z) = 2\bar{u}(\varphi, z)$, respectively. The resulting response is not so easy to predict from the above established rules.

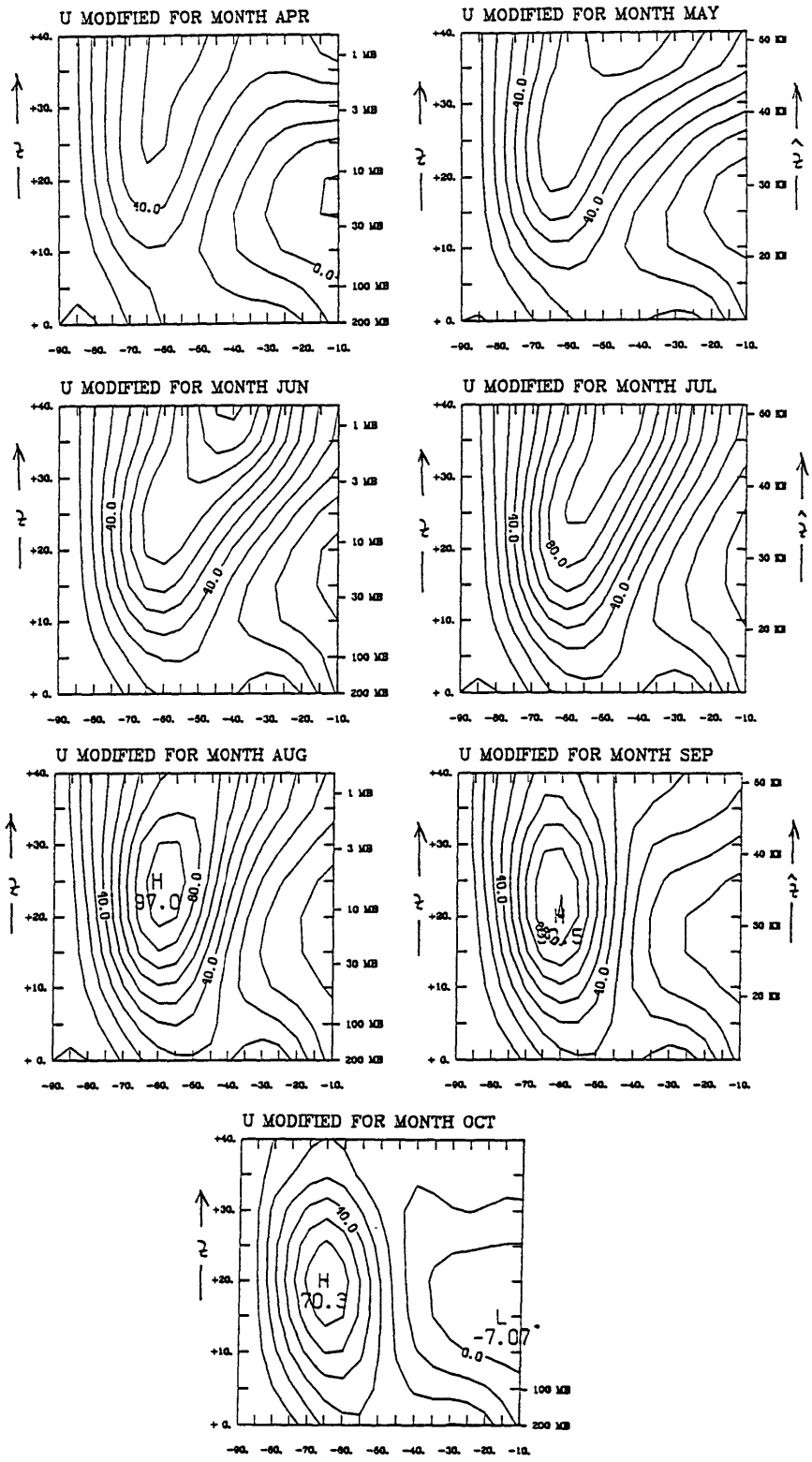

Figure 5.19: Modified basic state zonal wind (in m/sec) with locally stronger jet (see text for details). Contour interval: 10 m/sec. Meridional section. z and $\hat{z}$ in km, latitude in degrees.

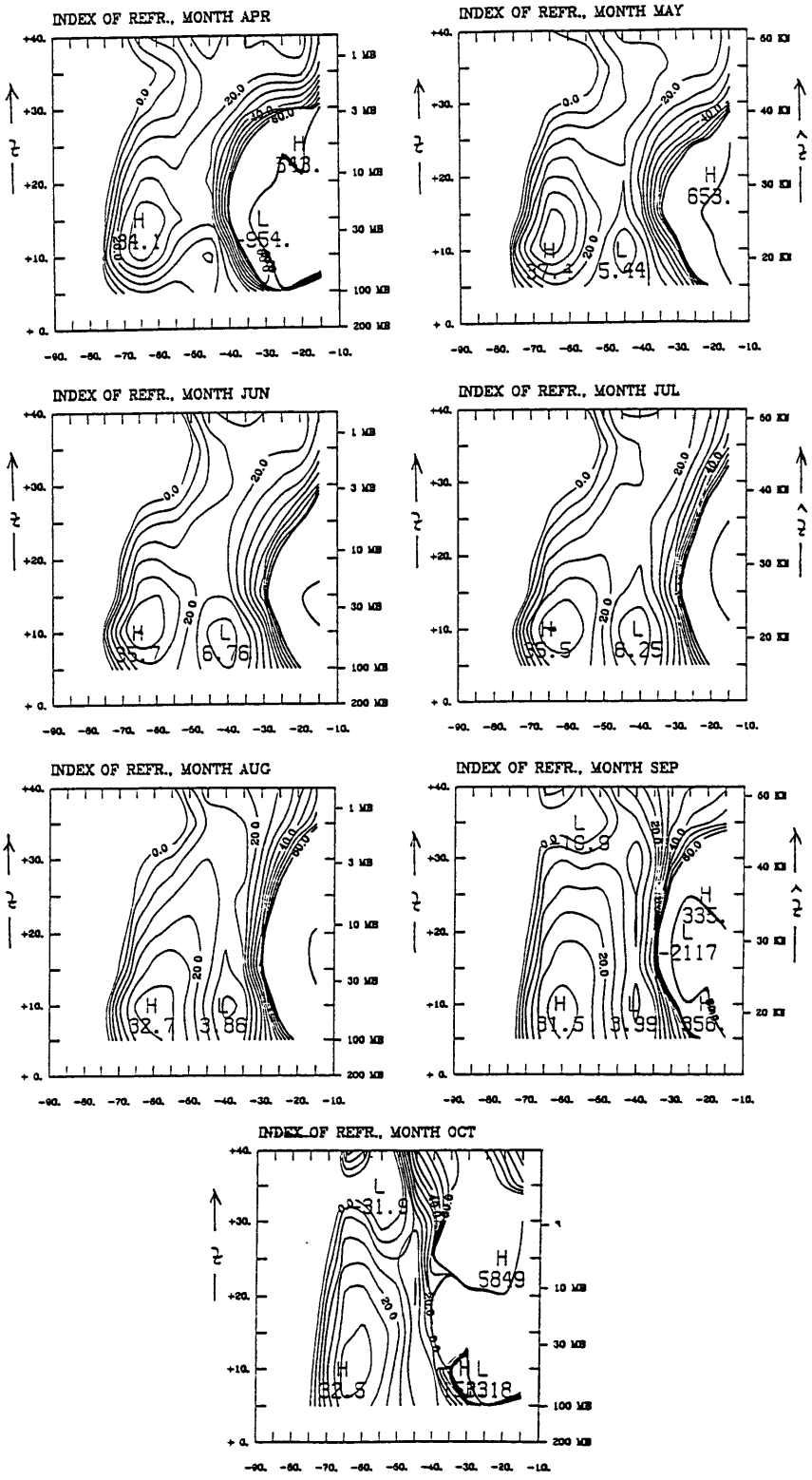

Figure 5.20: Refractive index for modified basic state with locally stronger jet (see text for details). Only contours between +0 and +60 are drawn. Contour interval: 5. Meridional section. z and $\hat{z}$ in km, latitude in degrees.

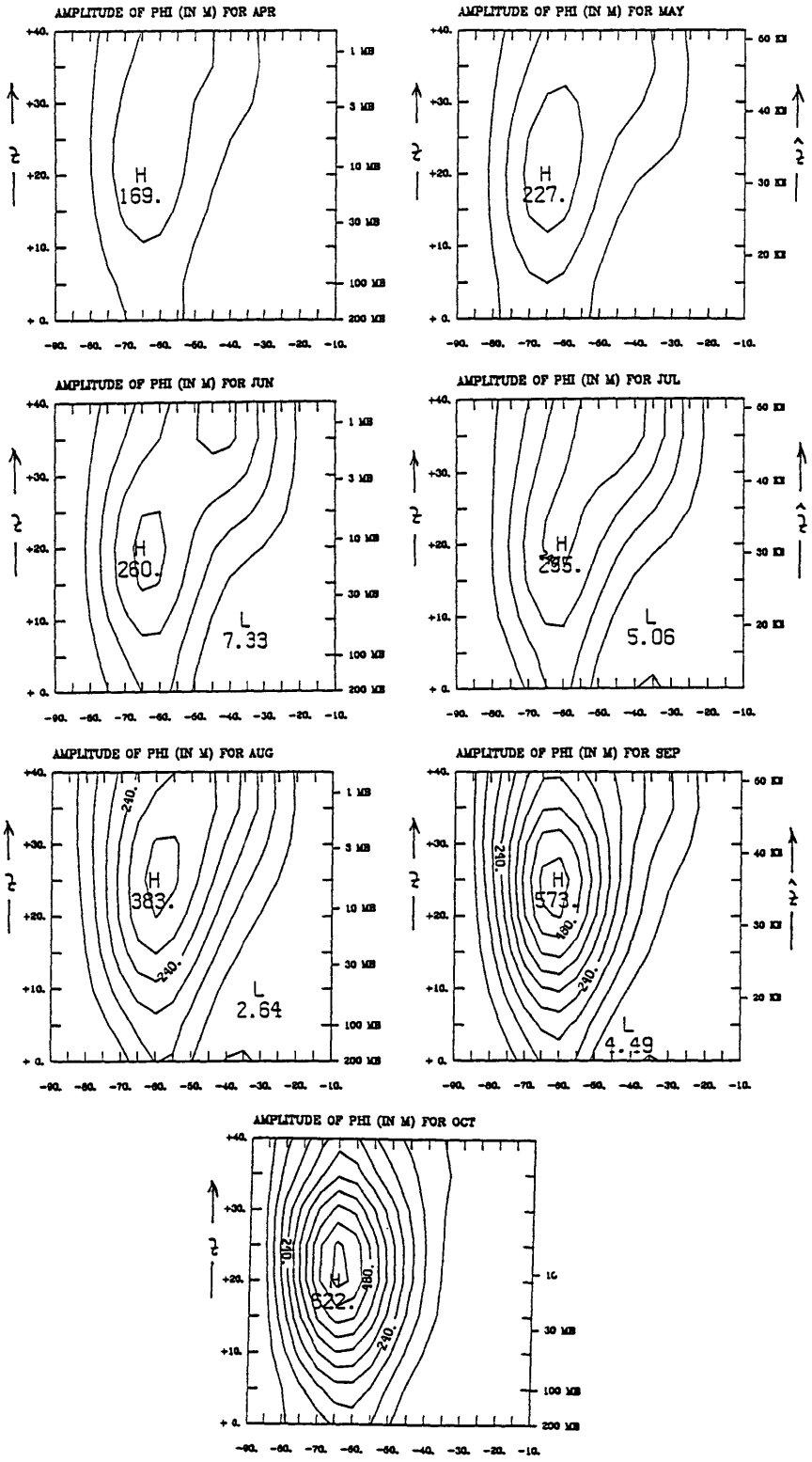

Figure 5.21: Wave amplitude (in geop. m) for for modified basic state with locally stronger jet (see text for details). Contour interval: 60 m. Meridional section. z and $\hat{z}$ in km, latitude in degrees.

Take for example the case $1/2 \times \bar{u}$. On the one hand weaker low level winds should lead to an increase in amplitude, on the other hand a substantially reduced jet in higher altitudes should rather lead to less of a response. The two effects to be superimposed act against each other. Still we can rationalize the result in terms of the refractive index.

We show here only the refractive index (figure 5.22) and the wave response (figure 5.23) for the two months June and July. In both the $1/2 \times \bar{u}$ and the $2 \times \bar{u}$ case the wave response is stronger than in the standard case. For $1/2 \times \bar{u}$ the refractive index is enhanced in low levels, whence wave propagation is facilitated in general. However, the wave guide structure gets somewhat lost, and in particular there is hardly any poleward gradient in refractive index in middle latitudes left. Even though the wave starts strongly, it is readily deflected towards the equator. The amplitude, therefore, shows a strong maximum in the middle stratosphere (around 10 mb). In the $2 \times \bar{u}$ case, the refractive index in low altitudes is lower than in the standard case. On the other hand, the wave guide structure is more pronounced. Therefore, there is less wave activity to start with, but what is left is guided upward more efficiently into higher altitudes. The result is a maximum in the higher stratosphere.

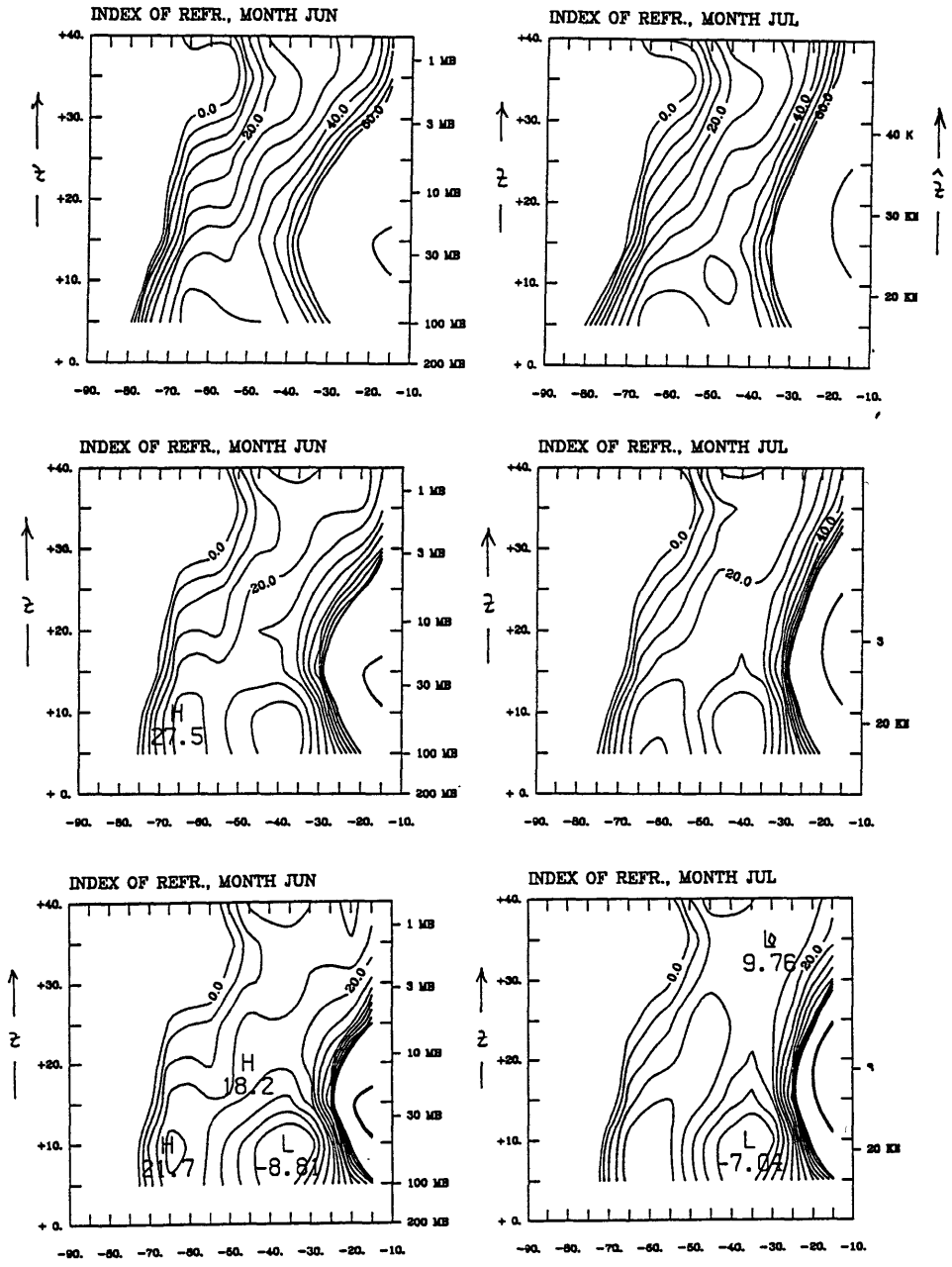

Figure 5.22: Refractive index for three different basic states: half of the original wind (upper row), standard case (middle row) and double the original wind (lower row). Only contours between +0 and +60 are drawn. Contour interval: 5. Meridional section. z and $\hat{z}$ in km, latitude in degrees.

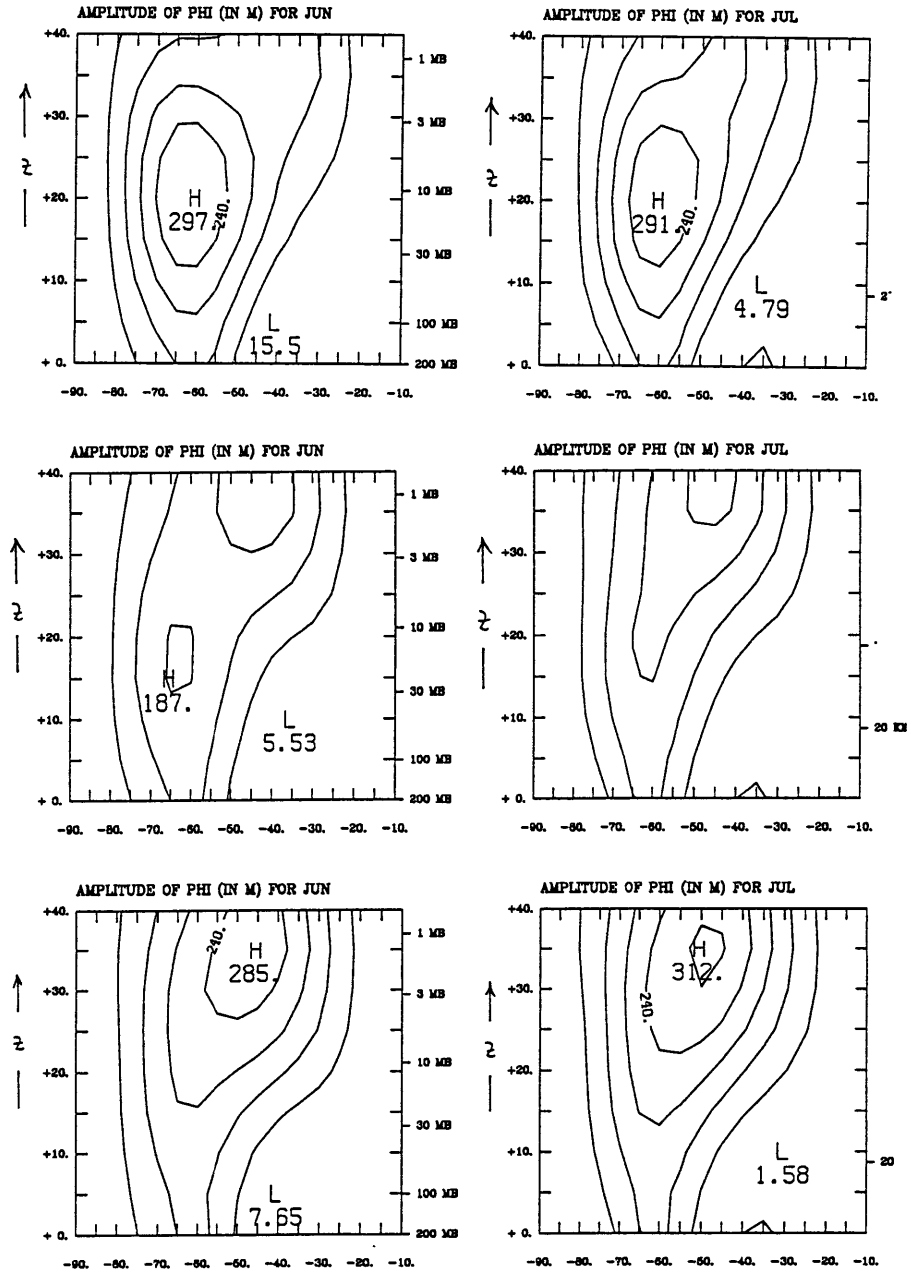

Figure 5.23: Wave amplitude (in geop. m) for three different basic states: half of the original wind (upper row), standard case (middle row) and double the original wind (lower row). Contour interval: 60 m. Meridional section. z and $\hat{z}$ in km, latitude in degrees.

Chapter 6

Summary and conclusions

Observations of stationary planetary waves in the southern stratosphere display a characteristic seasonal cycle with two maxima in early and late winter and a relative minimum in midwinter. As described in the introduction, previous observational and theoretical studies (Plumb, 1989a) suggest that wave-mean flow interactions are to a first approximation negligible in the Southern Hemisphere, and that the seasonal cycle of the waves is mainly determined by the transmission properties of the atmosphere. On the other hand, the refractive index, which is used to diagnose transmission properties of the atmosphere, does not reveal a very obvious seasonal cycle (Randel, 1988).

To investigate that issue, we set out to simulate the stationary wave 1 and its seasonal cycle with a hemispheric, linear, quasigeostrophic model, prescribing observed monthly mean zonal mean winds as the basic state and solving for the wave. Since the refractive index is a quasigeostrophic diagnostic, a quasigeostrophic model is adequate to study the relationship between this quantity and the waves. Moreover, the model is assumed to be realistic enough to capture the essential features of wave propagation.

The wave as resulting from the model was analyzed using the refractive index as a diagnostic, and it was compared with observations. Furthermore the model was used to study the sensitivity of the wave with respect to damping, forcing and basic state winds. We found good internal consistency of the model, but there was some unresolved discrepancy between the model results and the observations.

Summarizing the main results we want to emphasize the following points:

1. The *overall features* of stationary wave propagation are *reproduced satisfactorily* by the model. In agreement with the observations the wave amplitude generally grows with height in the lower stratophere, reaches a maximum and decreases above. The wave's phase displays a westward tilt with increasing height and latitude. EP flux directions indicate upward and equatorward wave propagation. The wave amplitude in the middle and upper stratosphere tends to mimic the basic state wind field. In particular the latitudinal location of the zonal wind maximum coincides well with the wave maximum, and the observed downward and poleward shift of the amplitude maximum towards the end of the winter is reproduced in the model.

2. We do not expect exact quantitative agreement between our simple model and the observations, but rather try to achieve a qualitative simulation. However, some of the *qualitative features*, which should be established well enough by observations to be considered real, are *not reproduced in the model.* In particular does the model not yield the observed *seasonal cycle* in wave amplitude with the characteristic relative minimum in midwinter. Instead, it gives a continous increase in wave amplitude throughout the winter season with a maximum in late winter (September and October). This has to be considered as a failure of the model. Also, the behaviour of the wave amplitude in a meridional cross section shows qualitative discrepancies between model and observations for some months.

3. Quite independent of the previous point, the model is *internally consistent.* By this we mean that the model wave (as opposed the observed wave) can be rationalized using model diagnostics. As by now well established through numerous studies (Matsuno, 1970; Karoly and Hoskins, 1982; Lin, 1982; Nigam and Lindzen, 1989), the wave propagation can be qualitatively diagnosed with the help of the refractive index. Particularly important features are its behaviour at low levels, a mid- to high-latitude ridge-like structure and a low level midlatitude minimum. Even though the refractive index *as a whole* does not vary dramatically through the winter season (Randel, 1988), the seasonal cycle of the model wave can

in fact be rationalized on the basis of considerable seasonal variations in these *particular features.*

Also the EP flux direction field shows consistent behaviour. However, it turns out to be a rather insensitive diagnosic for the climatological seasonal cycle and is therefore not very useful here.

4. Despite the failure to reproduce all observations with the model, the internal model consistency suggests that sensitivity studies are meanigful to some degree. Investigating the *sensitivity* of the model wave with respect to the *forcing*, we found that only mid- and high-latitude forcing substantially contributes to the higher stratospheric response. The amplitude field is qualitatively given through the basic state wind rather than through the exact form of the forcing. Also, the seasonal variation of the forcing (i.e. the wave amplitude at the 200 mb level) is much less than the wave amplitude variation in the higher stratosphere. Assuming that the wave amplitude in the higher stratosphere is entirely given through tropospheric forcing on one hand and upward propagation on the other hand,[1] we conclude therefore that the dominant factor causing the seasonal cycle in southern stratospheric stationary waves must be the variation in the wave propagation properties of the atmosphere.

5. Varying the *basic state wind* profile we find strong *sensitivity* of the wave response to low level wind changes and to changes which affect the narrowness of the jet structure. All those changes are accompanied by substantial changes in the refractive index, which, again, proves to be a useful diagnostic tool. This sensitivity might explain some of the quantitative discrepancies between model and observations. However, some qualitative differences remain, and in order to reproduce the observations in a "engineering type approach" one would have to modify the basic state in a rather unsystematic way.

The detected qualitative differences (item 2 above) between our model and the observations are presumably due partly to imperfectness of the observations (in connection with the mentioned sensitivity, item 5 above) and partly to imperfectness of the model. Possible model insufficiencies are:

[1]One might object that this concept neglects conceivable in situ generation of waves through instabilites. However, it is unlikely that such instabilities result in *stationary* waves.

- Quasigeostrophic theory as presented in chapter 3 is not exact enough in order to model the details of the present global wave dynamics. The use of a more involved primitive equation model as opposed to our quasi-geostrophic model would clarify this point.
- Critical levels might not act like absorbers, as assumed here, but partly or entirely like reflectors. Also, nonlinearity might be important. Both issues are hard to be dealt with in a linear model.
- The interannual variability (which is small, but existent) contributes to an error when using climatological monthly means. Also, it is not entirely clear how well the assumption of quasistationarity applies.

In the light of previous studies, and accounting for the specific properties of the southern stratospheric circulation, none of these model insufficiencies appear to be particularly grave. The question, what the main reason for the discrepancies between model and observations is, remains unresolved.

Thus, despite its consistency both internally and with previous studies, our model is not entirely conclusive concerning the explanation of the seasonal cycle of the southern stratospheric waves. Further research leading to the resolution of the above mentioned discrepancies would certainly provide new insight.

References

Andrews, D. G. (1989). Some comparisons between the middle atmosphere dynamics of the Southern and Northern Hemispheres. *Pure Appl. Geophys.* **130**, Nos. 2/3, 213–232.

Andrews, D. G., J. R. Holton, and C. B. Leovy (1987). Middle Atmosphere Dynamics. Academic Press.

Charney, J. G., and P. G. Drazin (1961). Propagation of planetary-scale disturbances from the lower into the upper atmosphere. *J. Geophys. Res.* **66**, 83–109.

Grose, W. L., and A. O'Neill (1989). Comparison of data and derived quantities for the middle atmosphere of the Southern Hemisphere. *Pure Appl. Geophys.* **130**, Nos. 2/3, 195–212.

Hartmann, D. L., C. R. Mechoso, and K. Yamazaki (1984). Observations of wave-mean flow interaction in the Southern Hemisphere. *J. Atmos. Sci.* **41**, 351–362.

Held, I. M. (1983). Stationary and quasi-stationary eddies in the extratropical troposphere: theory. *In:* Large-Scale Dynamical Processes in the Atmosphere. *Ed. by:* B. J. Hoskins and R. P. Pearce. Academic Press.

Hirota, I., T. Hirooka, and M. Shiotani (1983). Upper stratospheric circulations in the two hemispheres observed by satellites. *Q. J. R. Meteorol. Soc.* **109**, 443–454.

Karoly, D. J. (1989). The impact of base-level analyses on stratospheric circulation statistics for the Southern Hemisphere. *Pure Appl. Geophys.* **130**, Nos. 2/3, 181–194.

Karoly D. J., and B. J. Hoskins (1982). Three dimensional propagation of planetary waves. *J. Met. Soc. Japan* **60**, 109–123.

Killworth, P. D., and M. E. McIntyre (1985). Do Rossby-wave critical layers absorb, reflect or over-reflect? *J. Fluid Mech.* **161**, 449–492.

Leovy, C. B. (1984). Infrared radiative exchange in the middle atmosphere in the 15 micron band of carbon dioxide. *In:* "Dynamics of the Middle Atmosphere" (J. R. Holton and T. Matsuno, eds.), pp. 355–366. Terrapub, Tokyo.

Lin, Ben-Da (1982). The behaviour of winter stationary planetary waves forced by topography and diabatic heating. *J. Atmos. Sci.* **39**, 1206–1226.

Lindzen, R. S., and H. L. Kuo (1969). A reliable method for the numerical integration of a large class of ordinary and partial differential equations. *Mon. Wea. Rev.* **96**, 732–734.

Marks, C. J. (1989). Some features of climatology of the middle atmosphere revealed by Nimbus 5 and 6. *J. Atmos. Sci.* **46**, 2485–2508.

Matsuno, T. (1970). Vertical propagation of stationary planetary waves in the winter Northern Hemisphere. *J. Atmos. Sci.* **27**, 871–883.

McIntyre, M. E., and T. N. Palmer (1983). Breaking planetary waves in the stratosphere. Nature **305**, 593–600.

Mechoso, C. R., D. L. Hartmann, and J. D. Farrara (1985). Climatology and interannual variability of wave, mean-flow interaction in the Southern Hemisphere. *J. Atmos. Sci.* **42**, 2189–2206.

Nigam, S., and R. S. Lindzen (1989). The sensitivity of stationary waves to variations in the basic state zonal flow. *J. Atmos. Sci.* **46**, 1746–1768.

Palmer, T. N. (1982). Properties of the Eliassen-Palm flux for planetary scale motions. *J. Atmos. Sci.* **39**, 992–997.

Plumb, R. A. (1989a). On the seasonal cycle of stratospheric planetary waves. *Pure Appl. Geophys.* **130**, Nos. 2/3, 233–242.

Plumb, R. A. (1989b). Dynamics of the Middle Atmosphere. Lecture notes.

Press, W. H., B. P. Flannery, S. A. Teukolsky, and W. T. Vetterling (1986). Numerical Recipes. The Art of Scientific Computing. Cambridge University Press.

Randel, W. J. (1987a). Global Atmospheric Circulation Statistics, 1000–1 mb. NCAR technical note, NCAR/TN-295+STR.

Randel, W. J. (1987b). The evaluation of winds from geopotential height data in the stratosphere. *J. Atmos. Sci.* **44**, 3097–3120.

Randel, W. J. (1988). The seasonal evolution of planetary waves in the Southern Hemisphere stratosphere and troposphere. *Q. J. R. Meteorol. Soc.* **114**, 1385–1409.

Schoeberl, M. R., and M. A. Geller (1977). A calculation of the structure of stationary planetary waves in winter. *J. Atmos. Sci.* **34**, 1235–1255.

Simmons, A. J. (1974). Planetary-scale disturbances in the polar winter stratosphere. *Q. J. R. Meteorol. Soc.* **100**, 76–108.

List of Figures